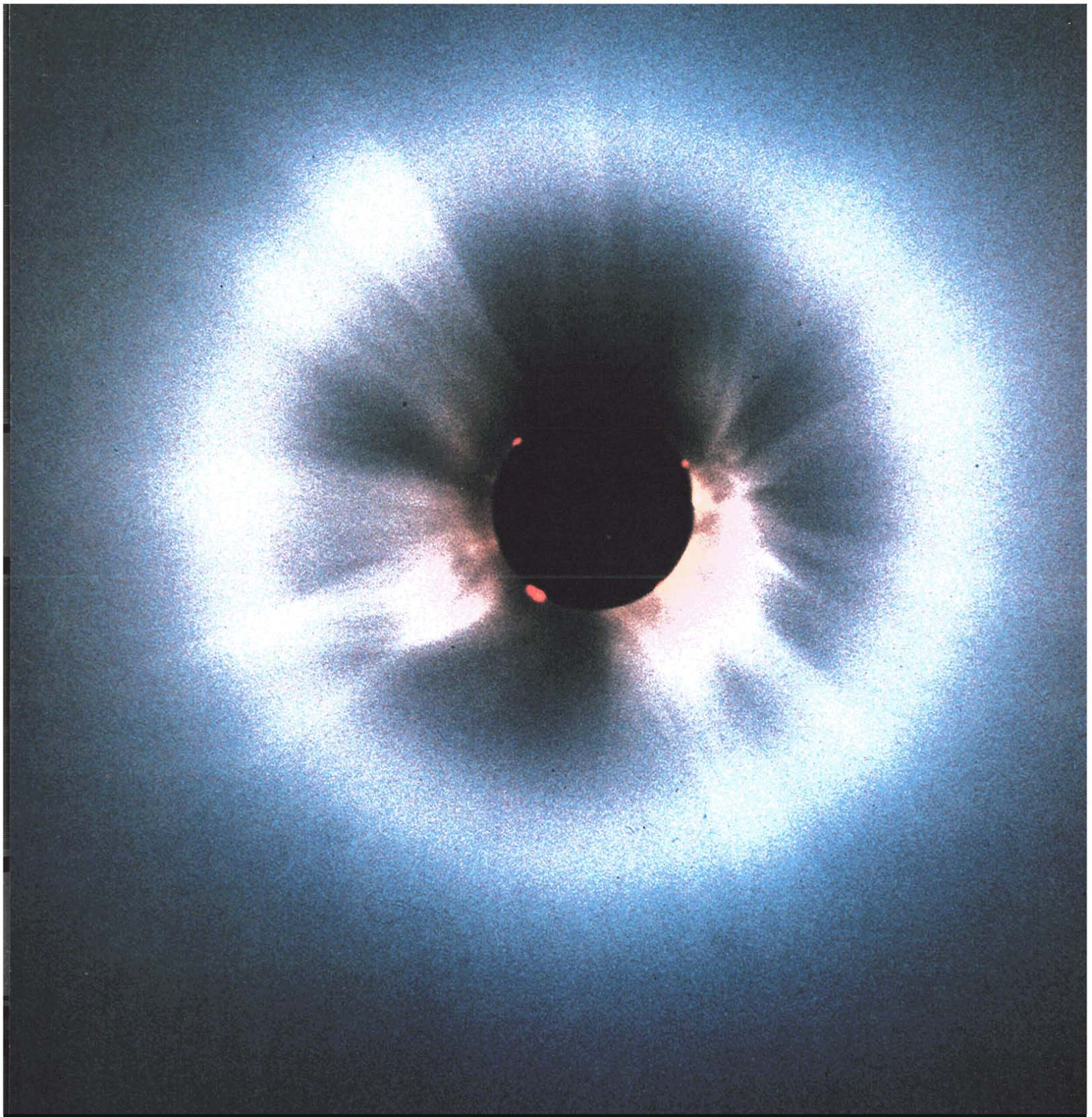

by Charles F. Keller and Donald H. Liebenberg

THE SOLAR CORONA AT TOTALITY

Airborne experiments probe the dynamic conditions of the sun's atmosphere during a total solar eclipse.

On February 16, 1980, the moon's shadow raced across our planet from the Atlantic Ocean to China at about 1600 kilometers per hour (Fig. 1). Thousands of spectators and scientists scattered along the shadow's path lifted their heads to glimpse the pearly glow of the solar corona, the sun's outermost atmosphere. Near the midpoint of this path where sun, moon, and earth were aligned for the longest time, a high-altitude United States Air Force jet made its carefully programmed rendezvous with the eclipse shadow. Aboard the aircraft were 18 Los Alamos scientists, observers from Indiana University and Kitt Peak National Observatory, a 12-man Air Force flight and support crew, a Kenyan observer, and two media representatives.

We were intent on recording the conditions in the solar corona during the second highest peak in solar activity in the past century. Five experiments, planned months ahead, were mounted inside the aircraft to make high-resolution measurements of coronal morphology, electron densities, electron temperatures, ion temperatures, and circumsolar dust rings. Our expedition was the seventh in a series of Los Alamos airborne missions that began in 1965 as an outgrowth of the national Test Readiness Program.*

During a total eclipse the aircraft provides near ideal conditions for observing the solar corona. At an altitude of 11 kilometers (36,000 feet) we enjoy freedom from cloud cover and reduced sky brightness and, by flying along the eclipse path, we increase the time of totality by 50% or more. In 1980, we had an unobstructed overhead view of the eclipse for 7 minutes 7 seconds while observers at the main ground site in India saw the event between clouds at a low angle in the afternoon sky for only 2 minutes 9 seconds.

This exceptional high-altitude platform outfitted with state-of-the-art instruments for tracking control and data acquisition (many of which derived from and contributed to the weapons testing program) has enabled Los Alamos to achieve many firsts in observation of coronal temperatures and densities. Such measurements are needed to resolve two major questions in coronal physics. How is the corona heated? And how is the solar wind generated?

We will look at what some of these measurements are and how they fit into study of the corona. We will also describe the technology developed at Los Alamos and how it has been used in carrying out these missions.

Early Coronal Studies

Total solar eclipses have been ob-

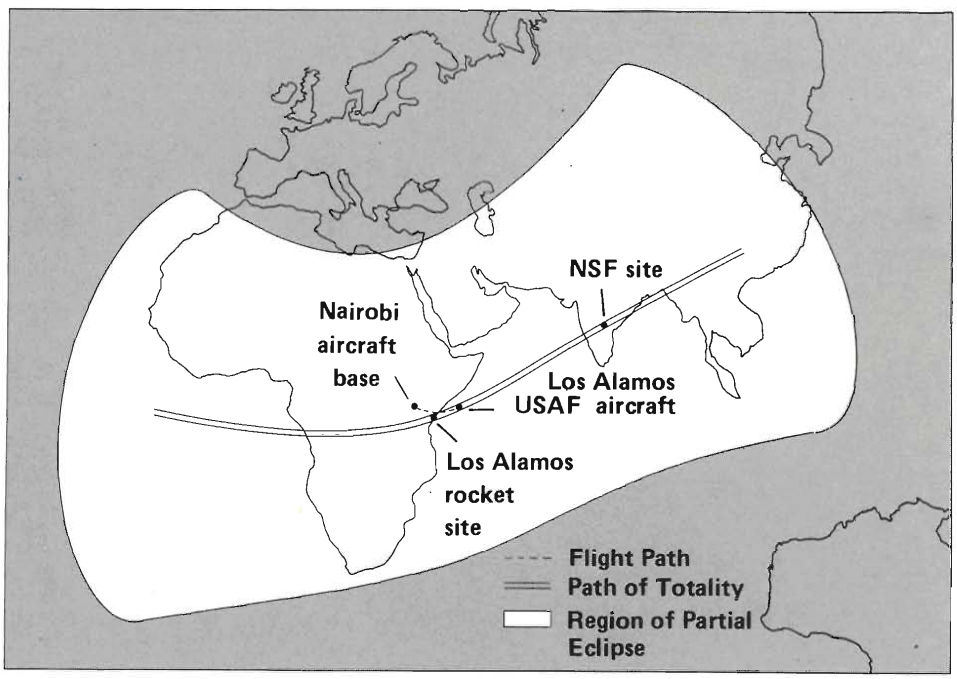

Fig. 1. The path of the moon's shadow first touched the earth in the Atlantic Ocean, then crossed Africa, the Indian Ocean, and India, and finally left the earth over China. Los Alamos observers launched rockets near Malindi, Kenya. The Los Alamos airborne expedition was based in Nairobi and flew to the point of longest totality duration just south of the equator over the Indian Ocean. The main ground-based scientific site was near Hyderabad, India.

*See "In Flight: The Story of Los Alamos Eclipse Missions" in this issue.

CORONAL MORPHOLOGY

Coronal morphology (depicted here out to 3 solar radii) is most likely shaped by the sun's magnetic field, which changes over an 11-year cycle of activity.

During a period of quiescence, coronal structure suggests that open lines of the sun's magnetic dipole field spread out from almost all solar regions except those near the equator, where the corona is brightest and fairly uniform. These regions of open field lines tend to be less bright and may qualify as coronal holes, features characterized by drastically reduced x-ray emission, low particle density, and possibly low temperature. It is known that, during periods of solar inactivity, coronal holes extend from the poles toward the equator and cover much of the sun's surface. Presumably solar wind flows strongly from coronal holes, thus depleting particle and energy densities. Polar plumes extend from the coronal holes at the sun's north and south poles.

During a period of maximum solar activity, as complex local magnetic fields develop over much of the sun's surface, the open dipole field lines and, with them, coronal holes appear to be restricted primarily to the polar regions. Many distinctive coronal features are formed as a result of this increased activity.

Perhaps the most striking feature is the helmet structure that extends outward into a long radial streamer at about 2 solar radii. The helmet is probably formed by magnetic field loops that rise from active regions of the photosphere. Charged particles are trapped along these field lines, but near 2 solar radii magnetic field strengths decrease sufficiently so that particles can drag the field lines radially outward to form a streamer.

Sunspots, prominences, filaments, and flares also form in active regions of the sun's surface. These regions seem to be confined to well-defined belts that move from high latitudes toward the equator as solar activity declines.

Coronal enhancements and condensations, bright areas near the sun's limb, are also associated with active regions. Their brightness is due to increased particle densities. An enhancement may persist for months, whereas a condensation may appear and disappear over a period of hours or days.

Changes in coronal morphology during the solar cycle are best portrayed by our image-enhanced photographs of the corona in the note "The Changing Corona" ■

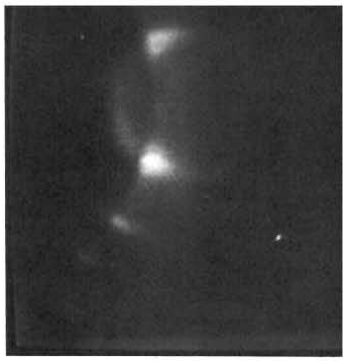

served for all of recorded time and probably since humans began to look at the sky, but the origin and nature of the sun's magnificent halo has baffled even the most astute observers. In 1605 Kepler attributed the display to a lunar atmosphere. Others associated it with the atmosphere of the earth or the sun. Not until the 1842 solar eclipse, when a spectacular display of corona and prominences was observed by astronomers in several European countries, was there general agreement on its solar origin.

The corona presented many puzzles, the most important being the absence of emission lines from hydrogen and helium and the presence of the coronal green line, a mysterious emission line that could not be identified with any known element on the sun. The green line was observed with a spectroscope by Harkness and Young in 1869. Originally this and other unidentified spectral lines were attributed to a new element named coronium. But there seemed to be no place for coronium in the periodic table, so the mystery of the spectral lines remained. Then in the late 1930s the lines were identified in the spectrum of Nova Pictoris, an exploding star whose atmosphere was known to be very hot. Finally in 1942, the great Swedish spectroscopist B. Edlen made laboratory measurements of hot plasmas and identified nearly all coronal emission lines as due to "forbidden" atomic transitions from highly ionized elements. The green line was produced by a transition in Fe XIV, an iron atom with 13 of its 26 electrons stripped away.* Other lines were attributed to other ionization states of iron, calcium, and nickel.

Tremendous energy is required to produce such highly ionized states. Also, for atoms to remain highly ionized long enough to deexcite through these forbidden transitions, the density must be very low. Thus the corona is a very hot plasma of ionized hydrogen, helium, and heavier elements with a temperature of a million degrees Kelvin or more (~1 MK) and a density one-trillionth the density of the earth's atmosphere. That the corona should be so hot was quite unexpected because it overlies the relatively cool surface of the sun (photosphere), which is about 6000 K.

What are the dynamics of this hot, rarefied atmosphere? How is it heated? How does it sustain itself when it is bounded below by the cool photosphere and above by the cold vacuum of interstellar space? The answers to these questions still remain quite tentative.

The Solar Wind

In the late 1950s the gross dynamics of the outer corona began to be understood. In 1957 Chapman noted that a simple model of the corona in hydrostatic equilibrium leads to a contradiction. According to such a model, the corona must extend to the earth's orbit and beyond. Its pressure must fall so slowly that at infinity the coronal pressure would be much too high to be balanced by the pressure of interstellar gas.

In 1958 E. Parker solved this problem by introducing the revolutionary and initially unpopular idea that the corona is not static at all, but instead is in a constant state of expansion. His model predicted a supersonic flow of particles out from the corona beginning at a few solar radii. This flow came to be known as the solar wind. Its existence was confirmed in the early 1960s when satellites first began to penetrate beyond the earth's magnetic field and detected particles traveling away from the sun at velocities of 400 kilometers per second. This variable stream of charged particles (mostly electrons and protons) is responsible for the sharp discontinuity of comet tails as they pass near the sun, a phenomenon first noted by L. Biermann in 1951. The solar wind also causes a variety of phenomena as it "blows" past the earth—from geomagnetic storms that interfere with radio communications to possible subtle effects on our weather causing climate variations that appear to be synchronized with the sun's magnetic activity cycles.

It is interesting that until now measurements of solar wind flow, interpreted through solar wind theory, have probably given as good an idea of the average conditions in the inner corona as direct observations. To match solar wind fluxes measured near the earth, these models predict that temperatures in the corona are maximum at about 2 $R_\odot$* and must decrease very slowly thereafter. In particular, if the temperature T falls off with radial distance from the sun as $(r/R_\odot)^{-b}$, then for all $0 \leq b < 1$, supersonic wind flow begins at a critical distance from the solar surface. Values of b may be estimated from observed particle fluxes. Beyond a few solar radii, collisions among particles and photons are so rare that ionization levels are "frozen in." In this collisionless plasma, temperatures refer to an average velocity distribution and do not imply local thermodynamic

Physicists refer to unionized iron as Fe I.

Distances from the center of the sun are commonly measured in units of the solar radius $R_\odot$ (~700,000 km); the limb of the sun is at 1 $R_\odot$

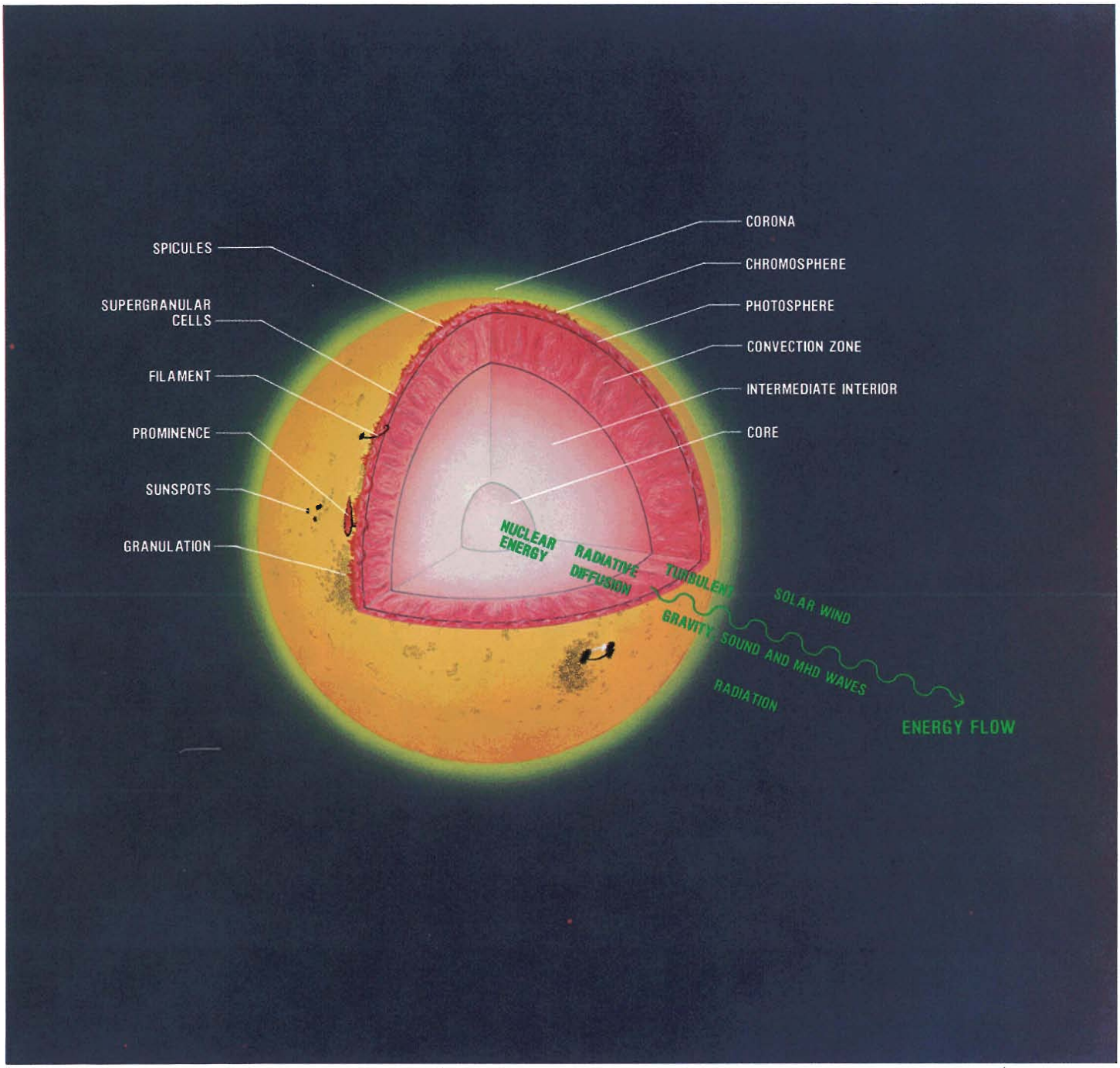

Fig. 2. Schematic depiction of the sun's radial structure and its atmosphere as well as modes of energy efflux. Radiative diffusion transports energy from the sun's core through the turbulent convection zone beginning at about 0.86 $R_{\odot}$. Convection cells in the turbulent layer are visible as a granulation pattern in the photosphere. The cells (about 1000 km in extent) form and disperse with lifetimes of a few minutes, and thereby produce 5-minute oscillations of the granulation layer that may be the source of acoustic waves. Another type of convection pattern called supergranulation is also observed in the photosphere. Large cells (10,000-100,000 km in extent) rise and spread out over a day or so. Supergranulation may produce a network of concentrated magnetic fields at the boundaries of supergranulation cells. This network exerts a strong influence on the upper atmosphere. It certainly shapes the corona and perhaps generates magnetic waves that heat the corona. The network of magnetic field lines is particularly complex in active regions where sunspots, filaments, flares, and prominences are formed.

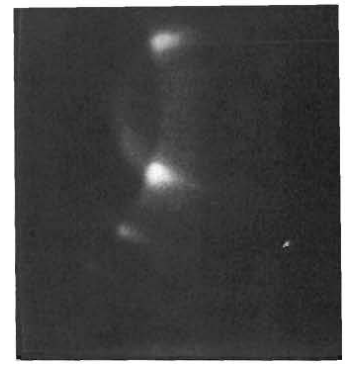

equilibrium.

Temperature measurements needed to confirm simple fluid models of solar wind flow have been in a state of confusion. Not only are these measurements very difficult to make but the corona is a complex, inhomogeneous structure that changes with time.

During 1973 and 1974, observations of the x-ray and extreme ultraviolet coronal spectrum from the Apollo Telescope Mount aboard Skylab revealed many facts about the inhomogeneous nature of the solar corona. One of the most important for solar wind theory was the existence of coronal holes, regions of low density, perhaps low temperature, and open magnetic field lines that are almost devoid of x-ray emission at the solar surface. At the time of the Skylab observations, when the sun was in a quiet phase, the hole regions extended down toward the equator. The very high velocity component of the solar wind observed during that time evidently emanated from the equatorial coronal hole region where particles stream out at high velocities along open field lines. However, the mechanism for accelerating these particles as well as the contributions to the solar wind from other regions of the corona are still not well known.

High-resolution data from our 1980 mission will help to determine the temperature structure in coronal holes and other coronal features and thus help to explain how the solar wind is generated in each of these areas.

Coronal Heating

Our 1980 data may also shed light on a problem that has puzzled solar physicists since the discovery of the hot corona. By what mechanism is energy from the photosphere deposited in the coronal plasma?

Radiation heating by the enormous flux of visible light emanating from the photosphere is ruled out because the coronal plasma is essentially transparent to visible wavelengths. We must look instead to mechanisms that could be produced by the interaction of mass motions and magnetic fields in the turbulent convection layers of the photosphere (Fig. 2).

Large volumes of gas constantly emerge from the surface, spread out and cool, and finally sink back into deeper layers of the photosphere. This convective energy could generate acoustic waves that propagate into the chromosphere and the extreme lower corona. Alternatively, magnetic waves generated by the interaction of convective cells with magnetic fields might provide a heating mechanism that extends far out into the corona. (Magnetic fields extend outward from the photosphere through the chromosphere and outward with the corona.)

This process might take place in very active regions of the solar surface. In these regions of high magnetic field strengths, we see eruptive prominences, filaments, and sun spots. Coronal condensations overlie these active regions. Perhaps as tangled loops of magnetic fields move around, currents flow that untangle field lines by reconnecting them in simpler configurations, thereby releasing large amounts of magnetic field energy in the form of magnetic waves. A similar but more extreme process is proposed for solar flares. Or perhaps magnetic waves are generated all over the sun's surface.

The details of these phenomena are too complicated to be modeled at present. But there are some questions we can hope to answer through observations. First, how far up in the corona is heat deposited? Is it all deposited in the transition zone between the chromosphere and the corona where the temperature rises from 0.01 to 1 MK in less than 1000 km? Or does the heating mechanism extend out to several solar radii, as suggested by solar wind theory? If so, how is energy transported through the corona?

Is energy distributed equally among electrons, or are protons heated preferentially by nonlinear processes, thus explaining why solar wind protons observed near the earth have higher temperatures? Finally, is solar wind flow a result of temperature gradients alone or are there mechanisms that accelerate the wind without heating it?

If acoustic waves are the major heat source, the lower coronal temperature would be maximum at approximately 1.1 $R_{\odot}$ because acoustic waves would be damped in the chromosphere or extreme lower corona. If magnetic waves are the major source, the temperature maximum would move farther out in the corona, possibly beyond 2 $R_{\odot}$, because magnetic waves would lose their energy much more gradually, possibly out as far as 25 $R_{\odot}$. Direct observations of this temperature maximum would obviously help to determine the mechanism of coronal heating. Also, direct observations of periodic variations in brightness would help to establish the existence of extended wave heating.

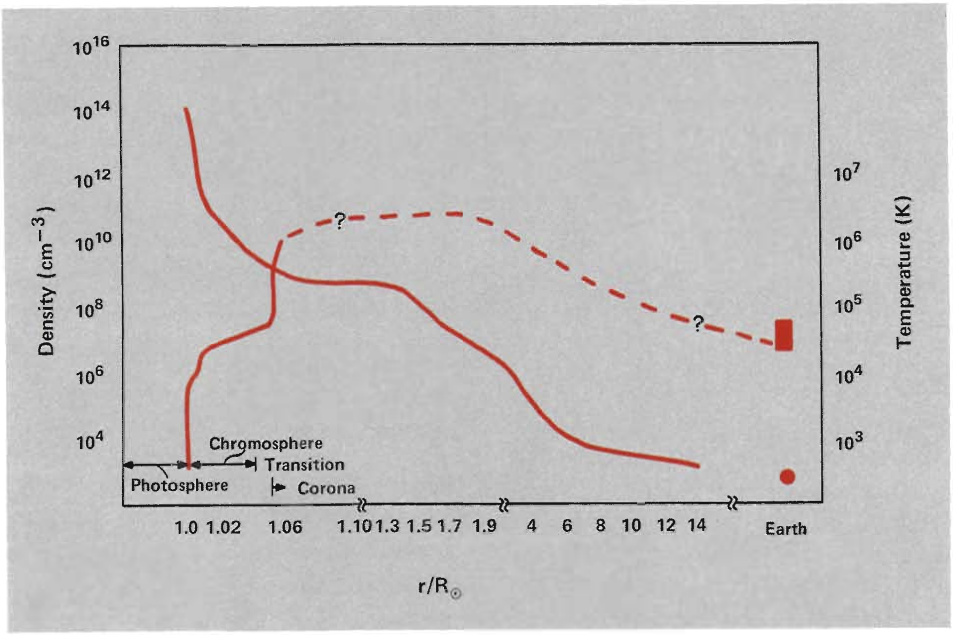

Fig. 3. Approximate variation of particle density and temperature as a function of radial distance. (Note radial distance scale changes.) The steep density decrease above the photosphere and the hundredfold increase in temperature from the base of the chromosphere to the corona are fairly well established but temperatures and gradients in the chromosphere and above are still the subject of research. The exact location of the steep temperature rise in the chromosphere-corona transition region is uncertain, although this region is known to be thin. Temperature and density values in the corona may vary from one feature to another and may be modified by the presence of prominences, flares, and active regions in the photosphere below. Temperature and density of the solar wind at the earth are shown for comparison.

The Problem of Coronal Temperatures

The key parameters for modeling energy transport in the corona are the distribution of electrons and ions in the corona and their temperature, or, more precisely, their velocity distribution.

The average values of the particle distribution are fairly well known, but the temperature distribution is not (Fig. 3). We would like to know not only gross averages but details of temperature distributions in various structural features of the corona since the energy transport will vary from one to another. At present the results from various methods gathered at various times are in disagreement. Although these discrepancies are understandable, given the fact that the various methods for measuring temperature involve different assumptions, the methods are complementary; if done in a coordinated fashion, the separate measurements can be compared to yield more information than any single one can yield alone.

HYDROSTATIC TEMPERATURES. Upper and lower limits on average coronal temperatures can be obtained from electron density measurements. The derivations for both limits assume that electrons and ions are in local thermodynamic equilibrium and electron density equals ion density at each point in the corona. The lower limit estimate is based on a model of the corona in hydrostatic equilibrium (neither expanding nor contracting). The pressure gradient exactly balances the acceleration of gravity,

$$\frac{dP}{dr} = -\rho \frac{g_\odot}{r^2} \quad , \qquad (1)$$

where P is pressure, r is radial distance from the center of the sun in solar radii, $g_\odot$ is acceleration of gravity at the sun's surface, and the material density ρ is directly proportional to the particle density n. Since coronal densities are low, we assume that the ionized gases obey the ideal gas law,

$$P = n k T \quad , \qquad (2)$$

which relates the pressure to the particle number n and temperature T. If we assume that the temperature is constant, we can derive the density variation with radial distance by differentiating Eq. (2) and substituting the result into Eq. (1). We obtain

$$\frac{dn}{n} \propto \frac{1}{T} \frac{dr}{r^2} \quad . \qquad (3)$$

Integrating Eq. (3), we find that a plot of log n versus 1/r is a straight line with a slope proportional to 1/T. Since the corona is nearly all hydrogen we may replace particle density with electron density, $n_e \sim n$. Consequently, if the experimental values of log n_e lie on a straight line, then the so-called hydrostatic temperature may be deduced from its slope.

Actual measurements of log n_e versus 1/r yield a straight line for $r \lesssim 2\ R_\odot$ with a slope corresponding to 1.4 to 1.6 MK. However in equatorial regions of the sun the slope changes between 3 and 5 $R_\odot$ and then beyond 5 $R_\odot$ it has a constant value corresponding to slightly less than 1 MK. This change in slope indicates that the corona does not have a constant temperature. Instead the temperature decreases with distance from the sun, a result consistent with an expanding rather than a static corona. Nevertheless, hydrostatic temperatures are useful as lower limits on average coronal temperature.

TEMPERATURES FOR AN EXPANDING CORONA. To determine temperatures for an expanding corona in, for example, a coronal hole, we add a velocity dependent term to Eq. (1).

$$\frac{dP}{dr} = -\rho \frac{g_\odot}{r^2} - \rho v \frac{dv}{dr} \quad , \qquad (4)$$

where v(r) is the radial expansion velocity. If we assume that the average solar wind mass flux κ is constant and equal to the value observed near the earth, we can obtain a rough estimate for the expansion velocity v from the relation

$$n_e(r)\ v(r)\ A(r) = \kappa\ , \qquad (5)$$

where A is the surface area. We then use the expansion velocity to determine the pressure gradient, dP/dr, from Eq. (4). Assuming that the pressure gradient is due to wave heating of the corona, we determine the temperature gradient from Eq. (2). Then, with a good value for the temperature from an independent measurement, we can use these temperature gradients to determine the variation of temperature with radius. When applied to the 1973 Skylab electron density data, this method yielded a steeply rising temperature curve for the coronal hole above the solar north pole.

OTHER CONSIDERATIONS. This result must be questioned for two reasons. First, since observed densities in coronal holes are very low, collisions may be so infrequent that local thermodynamic equilibrium cannot be assumed. A consequence would be that electron and ion temperatures are not the same. Second, the method assumes that pressure gradients, and thus the acceleration of the solar wind, are due to temperature gradients created by wave heating of the coronal plasma. However magnetic waves moving radially outward may accelerate the solar wind without heating it. Since Eq. (4) does not explicitly separate this nonthermal contribution to the velocity v(r), it yields effective pressures, and through Eq. (2), effective temperatures that are higher than the kinetic pressures and temperatures we are seeking. Temperatures derived from Eqs. (2), (4), and (5) must therefore be interpreted as upper limits. By considering these limits in conjunction with ion temperatures and velocity distributions determined from emission line measurements, it may be possible to separate thermal and nonthermal sources of solar wind acceleration.

EUV ION TEMPERATURES. Ion temperatures have been obtained from emission line measurements by two methods. One method is based on comparing measured and calculated intensities of resonance lines from allowed atomic transitions. These resonance lines are at extreme ultraviolet (EUV) wavelengths (Fig. 4). EUV data from 1 to 1.4 $R_\odot$ have been measured from satellites. Calculations assume an equilibrium model of coronal temperatures and densities and use known atomic parameters to determine the probability for resonance line emission. The assumed temperatures are adjusted to match measured and calculated line intensities. Errors are introduced by the crudeness of the assumed coronal model and by uncertainties in atomic parameters.

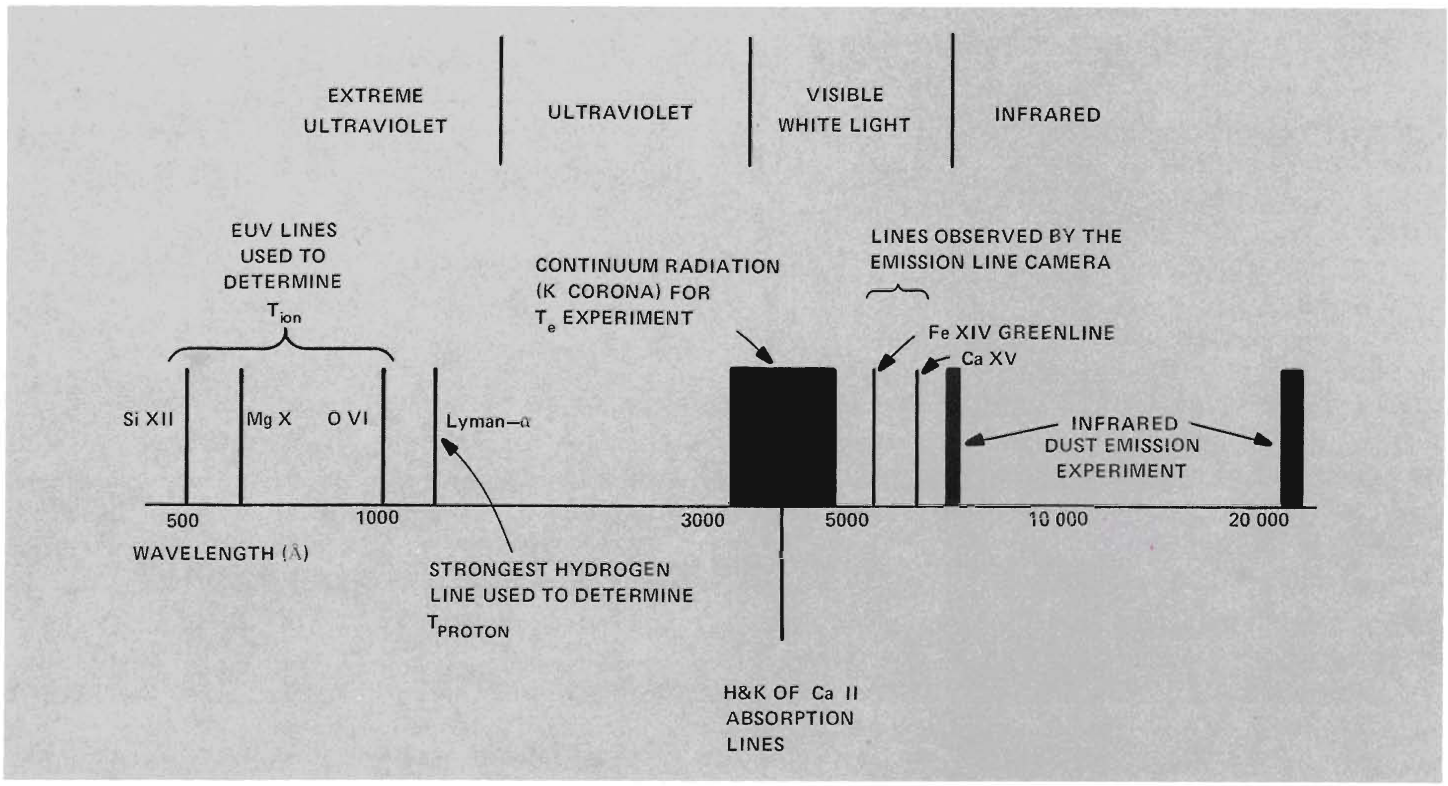

Fig. 4. Relative positions in the electromagnetic spectrum of observations made to determine coronal conditions. We do not attempt here to reproduce the actual coronal spectrum but merely indicate the wavelengths at which observations are made.

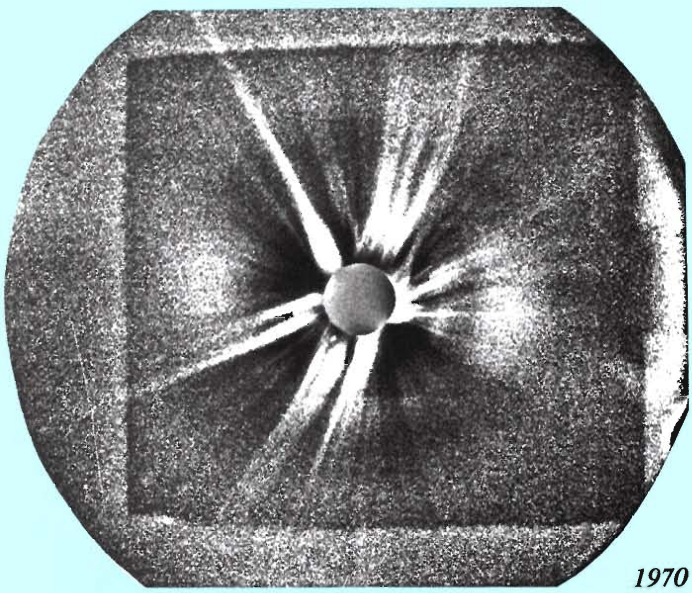

1970

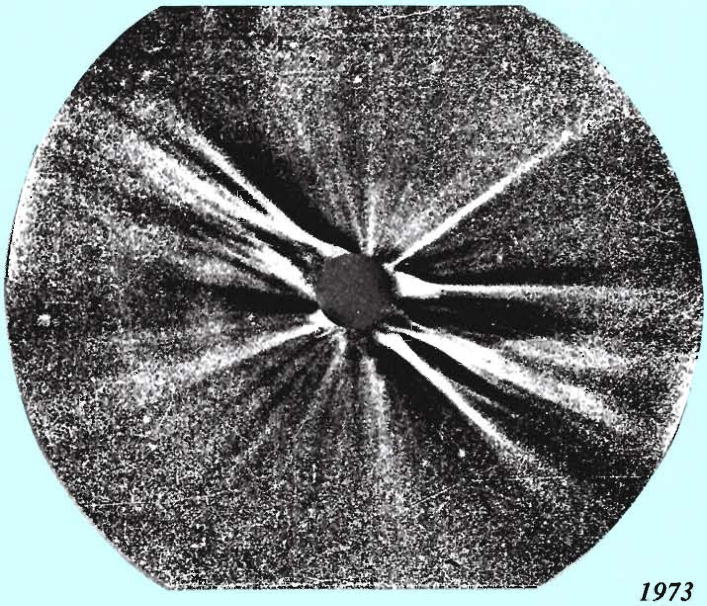

1973

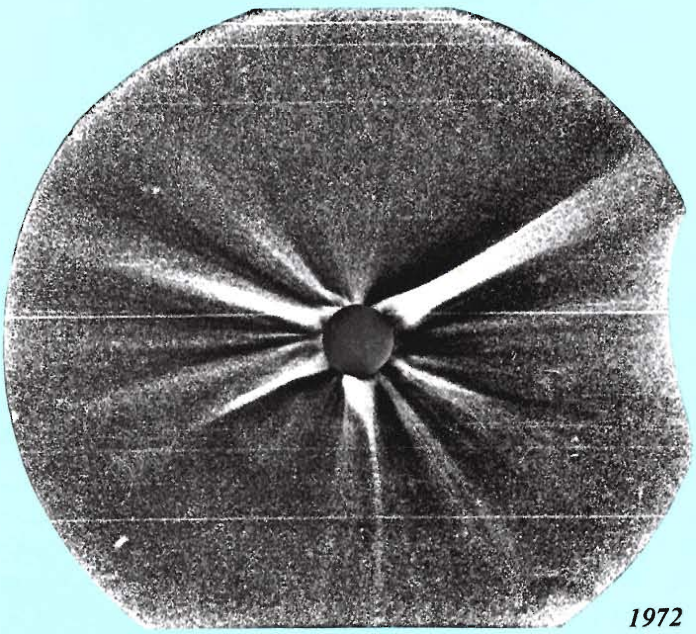

1972

THE CHANGING CORONA

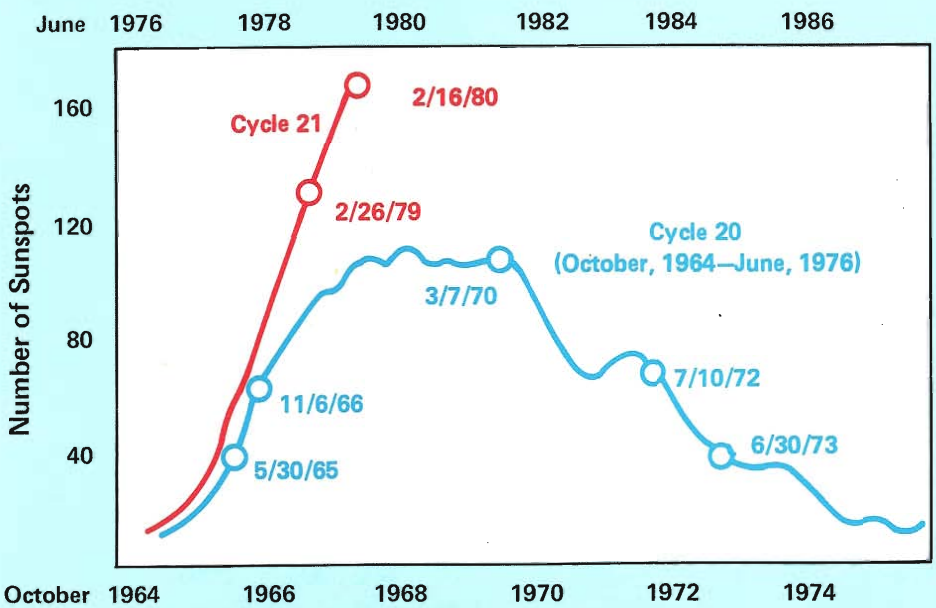

Portraits of the corona during five eclipses display its changing appearance as the sun passes through its cycle of magnetic activity. The eclipse dates are given on the accompanying graph of sunspot activity, which covers the present (red) and previous (blue) solar cycles. Each portrait is a composite of 20 to 30 photographic images taken from the NC-135 jet aircraft with the Laboratory-designed camera-polarimeter.

These portraits of the corona extending from the sun's limb to 12 solar radii are unparalleled. Photographs taken from the ground record only the inner corona to about 4 solar radii. Even Skylab's superb coronagraph can view

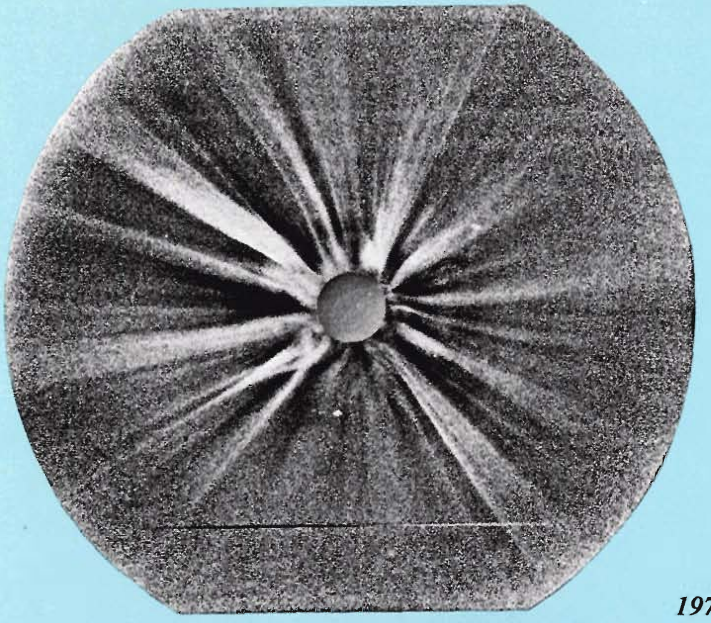

1979

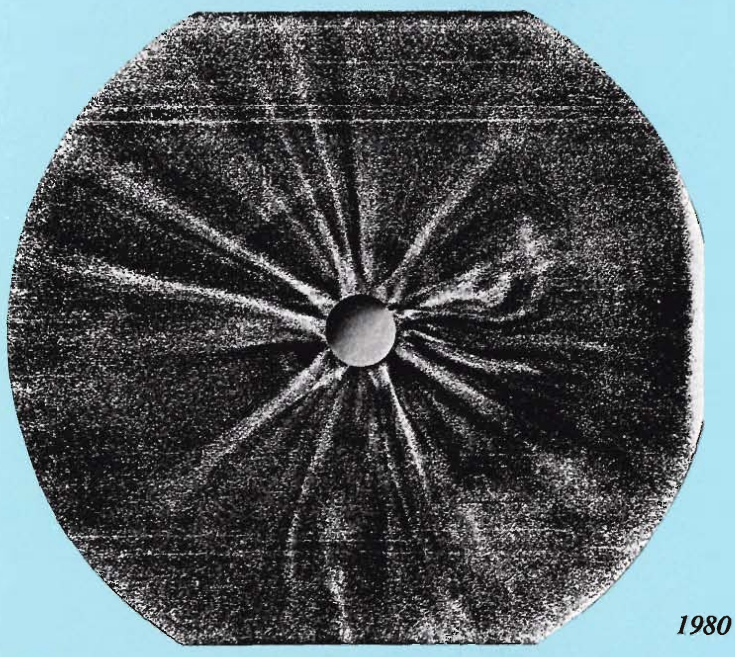

1980

only the region between 1.5 and 6 solar radii.

From this unique set of portraits, we can follow the evolution of streamers. The marked variation of the streamer pattern over the sun's 11-year activity cycle gives us a clear picture of the effect of solar activity on coronal structure and solar magnetic field.

The most striking structural change in the corona is the lack of bright streamers over polar regions during periods of low solar activity. At such times (1972 and 1973), polar coronal holes extend to lower solar latitudes. Solar wind flows from coronal holes and apparently bends the sun's magnetic dipole field strongly toward equatorial regions. During periods of high activity (1970, 1979, and 1980), streamers approach and often cover the polar regions and the dipole field is bent only slightly away from the poles.

Individual portraits bear careful study. Close to the sun, streamers are obviously dominated by magnetic fields. We see them twisted and curved in all directions. At larger distances, however, many streamers are seen to bend gradually back toward a radial direction, possibly under the influence of the expanding solar wind. Others remain nonradial even at the farthest distances. The information on streamer dynamics contained in these images awaits theoretical study ■

EMISSION LINE PROFILE ION TEMPERATURES. A somewhat more direct method involves the analysis of measured intensity versus wavelength profiles of emission lines from highly ionized iron and calcium. (Several emission lines have wavelengths in the visible spectrum.) The width of these Doppler-broadened emission lines is a direct measurement of ion kinetic temperatures, provided all the broadening is due to thermal motions. However mass motions and turbulence can also contribute to the broadening.

The Los Alamos line profile data out to 3 $R_{\odot}$ are the most extensive available. Our analysis suggests that ion temperatures deduced directly from the widths of heavy ion emission lines may be larger than kinetic temperatures by as much as 30% because of nonthermal contributions to the line broadening.

Kinetic temperatures may be deduced directly from the width of hydrogen's Lyman-α emission line at 1216 Å because nonthermal contributions to the line broadening are proportionally much less than for heavier mass ions. Since Lyman-α radiation cannot penetrate our atmosphere, such measurements must be made at altitudes of 100 km or greater. Data between 1.5 and 3 $R_{\odot}$ are now available from rocket-borne experiments performed by scientists from Harvard University and the High Altitude Observatory of the National Center for Atmospheric Research.

The results of recent temperature measurements shown in Fig. 5 are in obvious disagreement. In coronal holes (Fig. 5a), we see upper and lower limits on kinetic temperatures based on electron density data. The lower limit is ~1

MK based on the assumption of a static, isothermal corona. The Skylab electron density data, interpreted through a model that accounts for expansion velocities as described above, results in a steeply rising curve that reaches 3.5 MK by 3 $R_\odot$. The other three observations fall within these bounds but are too sparse to allow determination of the position of the temperature maximum. The single EUV temperature and the single Lyman-α proton temperature suggest extended magnetic heating. When the Los Alamos iron ion temperatures are included, the temperature maximum moves below 1.3 $R_\odot$.

Figure 5b shows similar results for relatively quiet regions of the corona (regions that are devoid of obvious streamers but are not coronal holes). Neglecting the iron ion temperature puts the temperature maximum beyond 1.4 $R_\odot$; including it moves the maximum below 1.2 $R_\odot$. Preliminary iron ion temperatures from the Los Alamos 1973 eclipse observations show ever increasing temperatures down to 1.1 $R_\odot$. If the electron density and the EUV results in the lower corona can be believed, then the iron ion results must include a large turbulent contribution to line broadening.

Interpretation of the results shown in Fig. 5 is further complicated by the fact that the data were obtained at different times and at different places in the corona. To resolve the discrepancies, we need simultaneous observations of ion temperatures, electron temperatures, and electron densities. One of the primary goals of the Laboratory's 1980 solar eclipse expedition was to do just this.

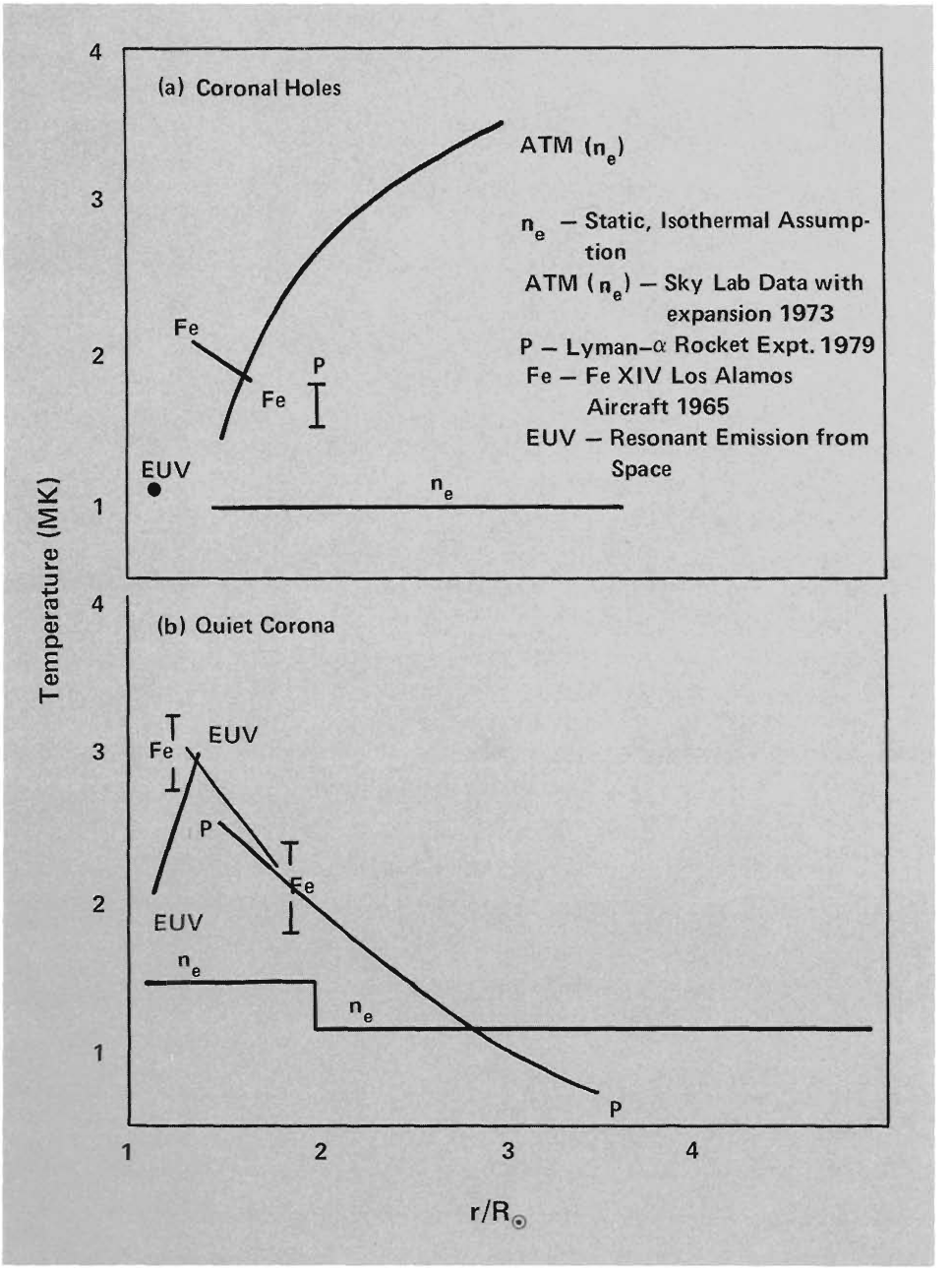

Fig. 5. Plots of coronal temperature versus radial distance for (a) coronal holes and (b) a quiet coronal region. As discussed in the text, data are sparse and, when compared, confusing. The main purpose of the Los Alamos expedition was to attempt to reduce some of the sources of disagreement by making cotemporal and cospatial measurements.

The 1980 Experiments

The sun's magnetic activity follows a well-known 11-year cycle becoming very active, waning to near total inactivity, and then repeating. The amplitude of this variation is never the same, but by 1979 it was obvious that the 1980 maximum would be one of the highest in history and many experiments were planned to observe the solar corona during the eclipse in February, 1980.

The National Aeronautics and Space Administration (NASA) planned to launch the Solar Maximum Mission, a satellite similar to Skylab's observatory. Aboard it would be experiments to determine electron densities and to obtain a crude estimate of ion temperatures from Fe XIV emission intensities. (Unfortunately this experiment was not operating by the time of the eclipse.) NASA also funded two rocket experiments, including one from Los Alamos, to measure proton temperatures from the Lyman-α line. The Naval Research Laboratory's orbiting coronagraph was to make hourly recordings of the white light from the outer corona (3-10 $R_\odot$). The National Science Foundation (NSF) planned to send to India a large contingent of ground-based observers, who would make a variety of measurements.

In planning the Los Alamos airborne

expedition, we were in communication with scientists from NASA projects and some NSF projects. It was apparent that cross-calibration and data comparison would assure maximum confidence in the results.

As discussed above, to answer significant questions about the nature of coronal heating and solar wind acceleration requires simultaneous measurements of the following:

- electron density, n_e
- ion temperature, T_{ion}
- electron temperature, T_e.

All these measurements were attempted by our expedition. All were designed to provide good two-dimensional spatial resolution. We expected to be able to determine all the quantities not only in the relatively uniform portions of the corona, but also within major features such as streamers, condensations, and coronal holes. Table I summarizes the experiments and the information sought.

To determine ion temperatures we measured the Doppler-broadened emission lines from two heavy ions—Fe XIV and Ca XV. We will compare our results with proton temperatures de-

TABLE I

1980 Solar Eclipse Experiments

Experiment	Principal Investigators[a]	Information Obtained or Sought	Resolution
Emission Line Ion Temperature Measurement of coronal Fe XIV and Ca XV emission line profiles with Fabry-Perot interferometer	D. H. Liebenberg E. A. Brown R. N. Kennedy H. S. Murray W. M. Sanders	Temperatures of Fe XIV and Ca XV, variation of emission line intensity with radial distance, and nonthermal contributions to ion temperature from 1 to 3 $R_\odot$	0.005 $R_\odot$ (3500 km)
Electron Temperature Measurement of K coronal spectral intensity with silicon photodiode detector array	M. T. Sandford F. J. Honey R. K. Honeycutt, Indiana University	Electron temperature and coronal spectra at 1.2, 1.6, and 2.0 $R_\odot$	0.067 $R_\odot$ (46,000 km)
Electron Density Measurement of intensity and polarization of coronal light with camera-polarimeter	C. F. Keller J. A. Montoya B. G. Strait	Electron density, K + F corona intensity, and K corona polarization from 1.1 to 5 $R_\odot$ in polar regions and from 1.1 to 12 $R_\odot$ in equatorial regions and image-enhanced photographs of streamers from 1 to 20 $R_\odot$	0.067 $R_\odot$ (46,000 km)
Photography Coronal photography with radially graded filter and internal occulting disc	W. H. Regan C. G. Lilliequist	Detailed coronal structure from 1 to 6 $R_\odot$	0.033 $R_\odot$ (23,000 km)
Infrared Emission of Dust Rings Measurement of coronal infrared emission intensity with InSb detector and charge-injection-device television camera	J. P. Mutschlecner R. R. Brownlee D. N. Hall, Kitt Peak National Observatory	Radial location of dust rings and infrared emission intensity from 2 to 50 $R_\odot$	0.25 $R_\odot$ (175,000 km)

[a] *Unless otherwise indicated, the investigator is affiliated with Los Alamos. Other Laboratory personnel contributing to the 1980 solar eclipse expedition were W. H. Roach (scientific commander), R. A. Jeffries (in charge of liaison with the USAF), D. H. Collins (logistics officer), C. T. Barnett (movie photographer), and J. S. Martinez (still photographer).*

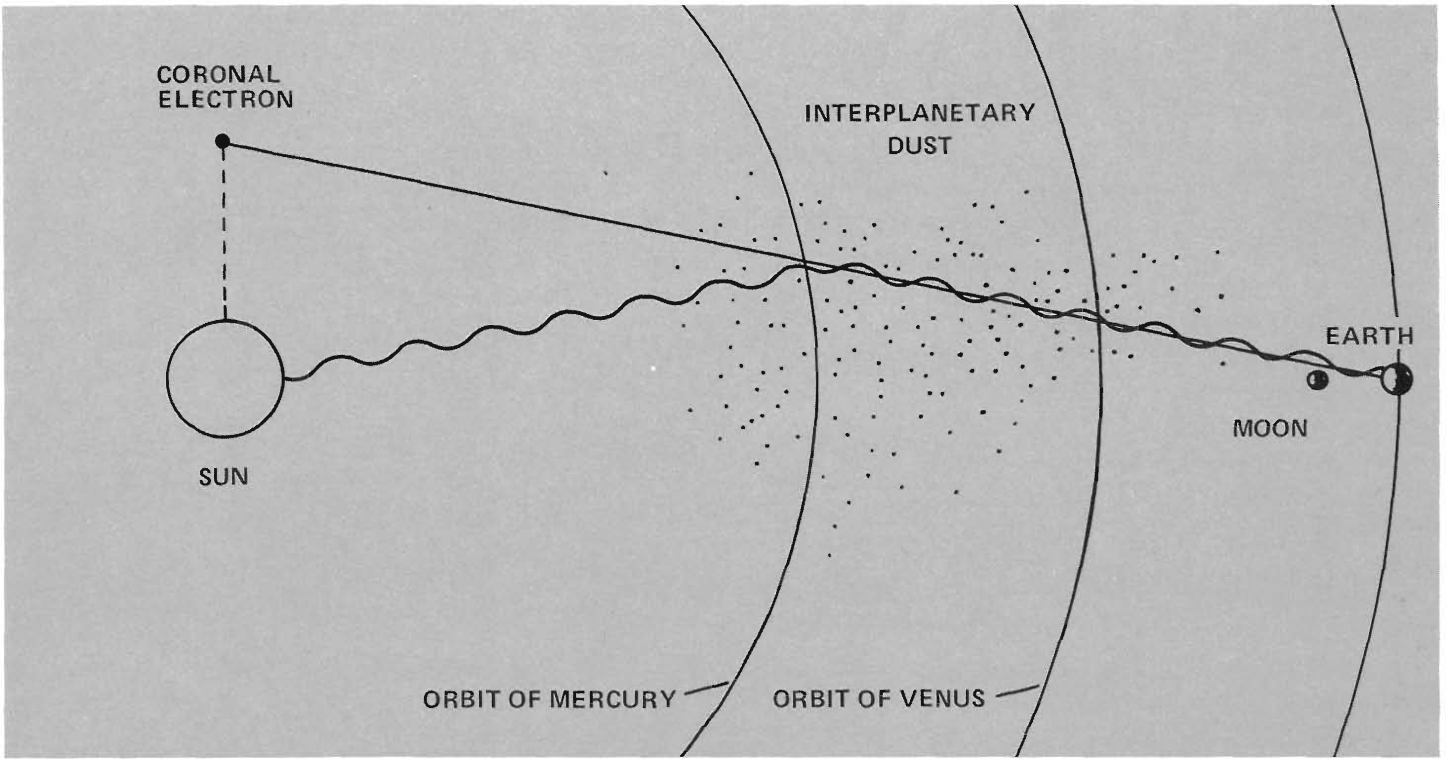

Fig. 6. The white light we observe during a total solar eclipse has two components, light from the photosphere scattered to us by electrons in the corona (straight line) and light from the photosphere scattered to us by interplanetary dust (wavy line).

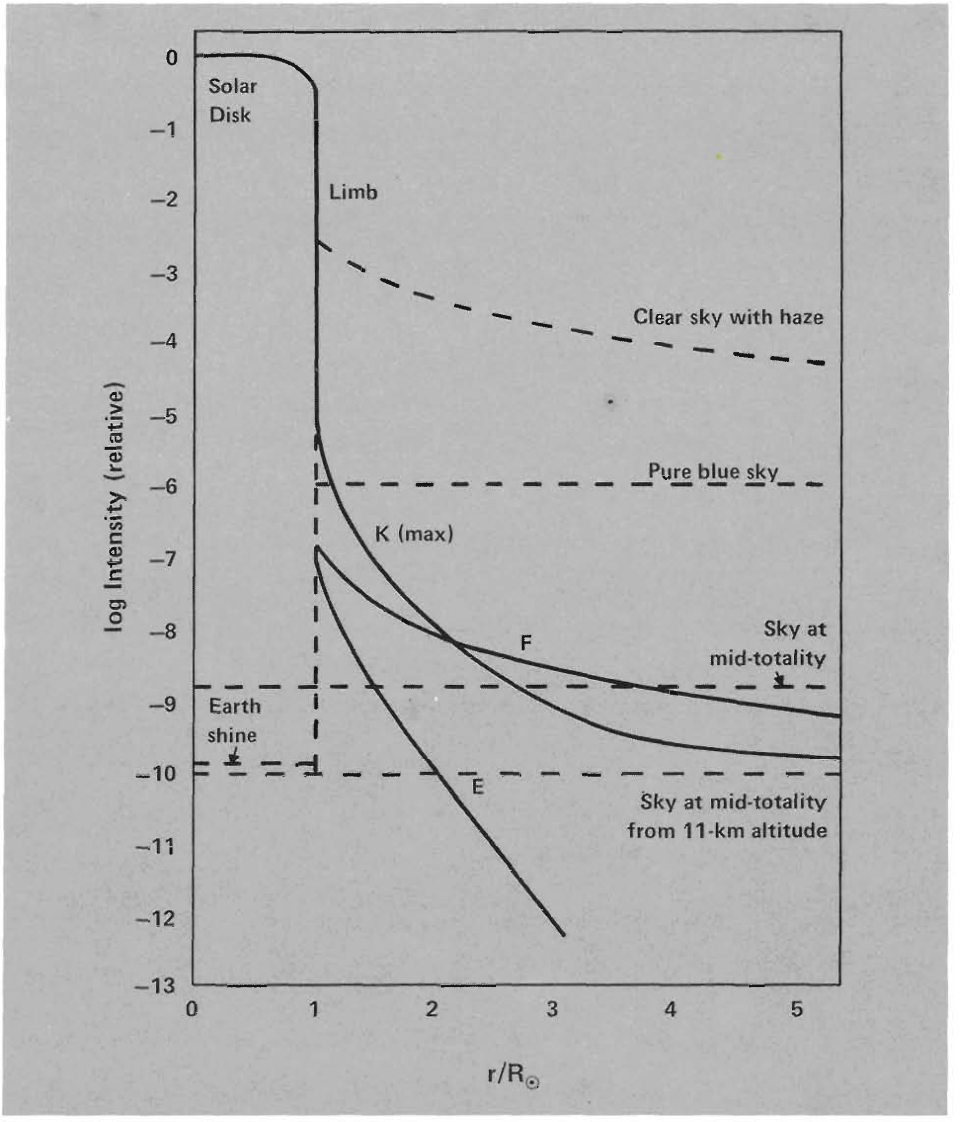

Fig. 7. Relative intensity of components of coronal light as a function of radial distance. The K corona is continuous light from electron scattering. The F corona is light from dust scattering. E is the combined light of emission lines. Relative background intensities under various observation conditions are also shown. Note the tenfold reduction in sky background intensity for high-altitude observations over ground-based observations.

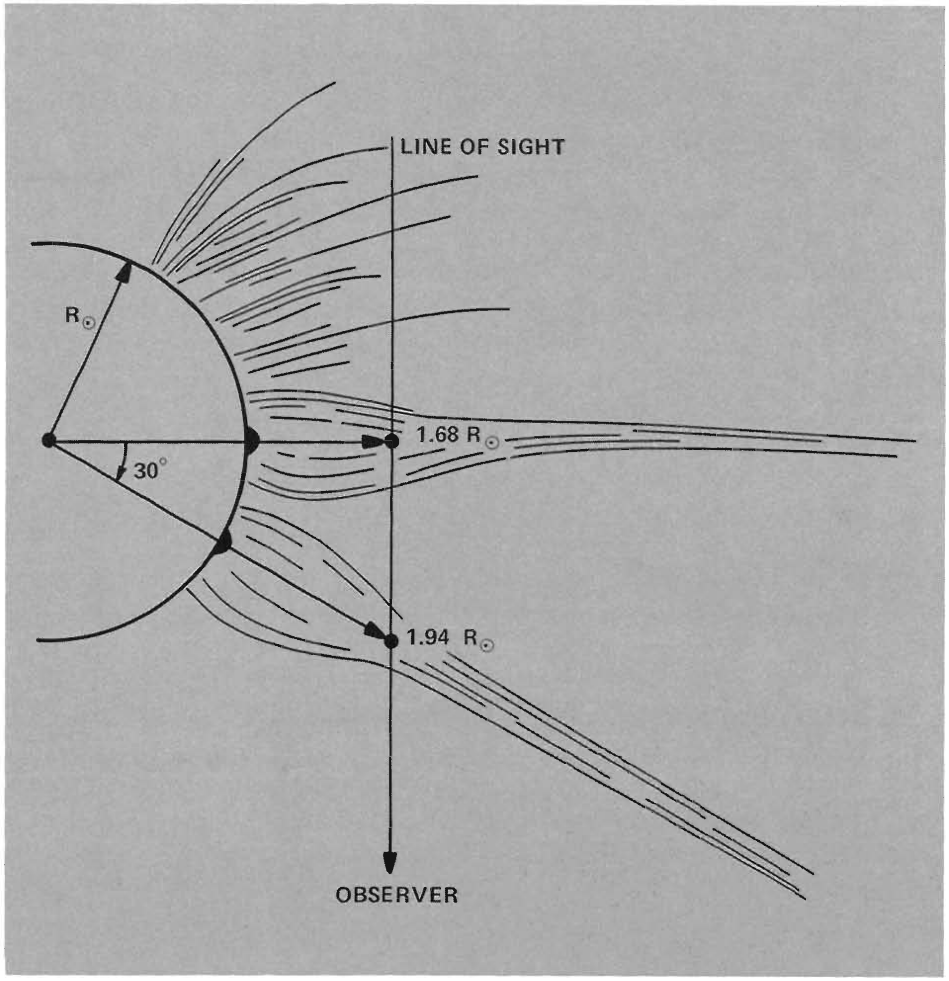

Fig. 8. Eclipse observations of the corona are made along a line of sight, but in many cases single coronal features can be identified reliably. This is because features closer to the limb are more intense and therefore contribute more light to the measured signal. For example, the line of sight shown here intercepts a streamer in the plane of the sky at 1.68 $R_\odot$ and an identical streamer 30° out of the plane of the sky at 1.94 $R_\odot$. The streamer in the plane of the sky contributes about 2.5 times as much white light and about 5.5 times as much emission line intensity to the observed signal as does the streamer out of the plane of the sky.

duced from rocket measurements of Lyman-α emission at several points in the corona beyond 1.5 $R_\odot$ to distinguish thermal from nonthermal contributions to line broadening. We are particularly interested in determining whether the extremely high ion temperatures at the base of the corona deduced from our 1973 results are correct or should be attributed to the effects of turbulence, but we must await data from these low altitudes. We also measured electron densities, recorded high-resolution images of the corona, and attempted to observe electron temperatures by a new, untried method. Finally, we attempted to determine the location of hot dust rings around the sun from their infrared emissions.

Except for the data loss from a mechanical failure in the electron temperature experiment, we obtained excellent data in all areas. And photographs of the corona taken from the aircraft will enable us to associate our detailed observations with particular spatial structures.

Data reduction and comparison is a long and difficult process that is only beginning. Before we discuss each experiment and give an early estimate of the data it acquired, let us consider some of the general conditions of coronal observation.

Observing the Corona

The angular sizes of the moon and the sun, as seen by an observer on (or near) the earth are approximately equal. During a total eclipse, this fortuitous circumstance enables us to view the solar corona, a region otherwise obscured by the intensity of the photosphere. Coronal light comes from several sources, the most intense being light from the photosphere that has been scattered by particles in the corona. This white light consists of two components, the K corona—sunlight scattered by electrons—and the F corona—sunlight scattered by dust grains (Fig. 6). Superimposed on these spectral continua are emission lines from highly ionized heavy ions. Figure 7 displays the relative intensities of the various components of coronal light; these intensities are compared with the brightness of the sky under various observational conditions. Note the sharp reduction in sky brightness during a solar eclipse. Although emission line intensities are much less than white light intensities, they are clearly visible above the white light background when observations are limited to very narrow wavelength bands. However, the rapid decrease of emission line intensity with radial distance from the sun makes measurements impossible beyond 3 $R_\odot$ with present instrumentation.

Apart from the signal intensity, the other unalterable limitation on observations is geometry—we can only record two-dimensional information about three-dimensional objects. As shown in Fig. 8, every observed signal is integrated along a line of sight through the corona. If the corona were spherically

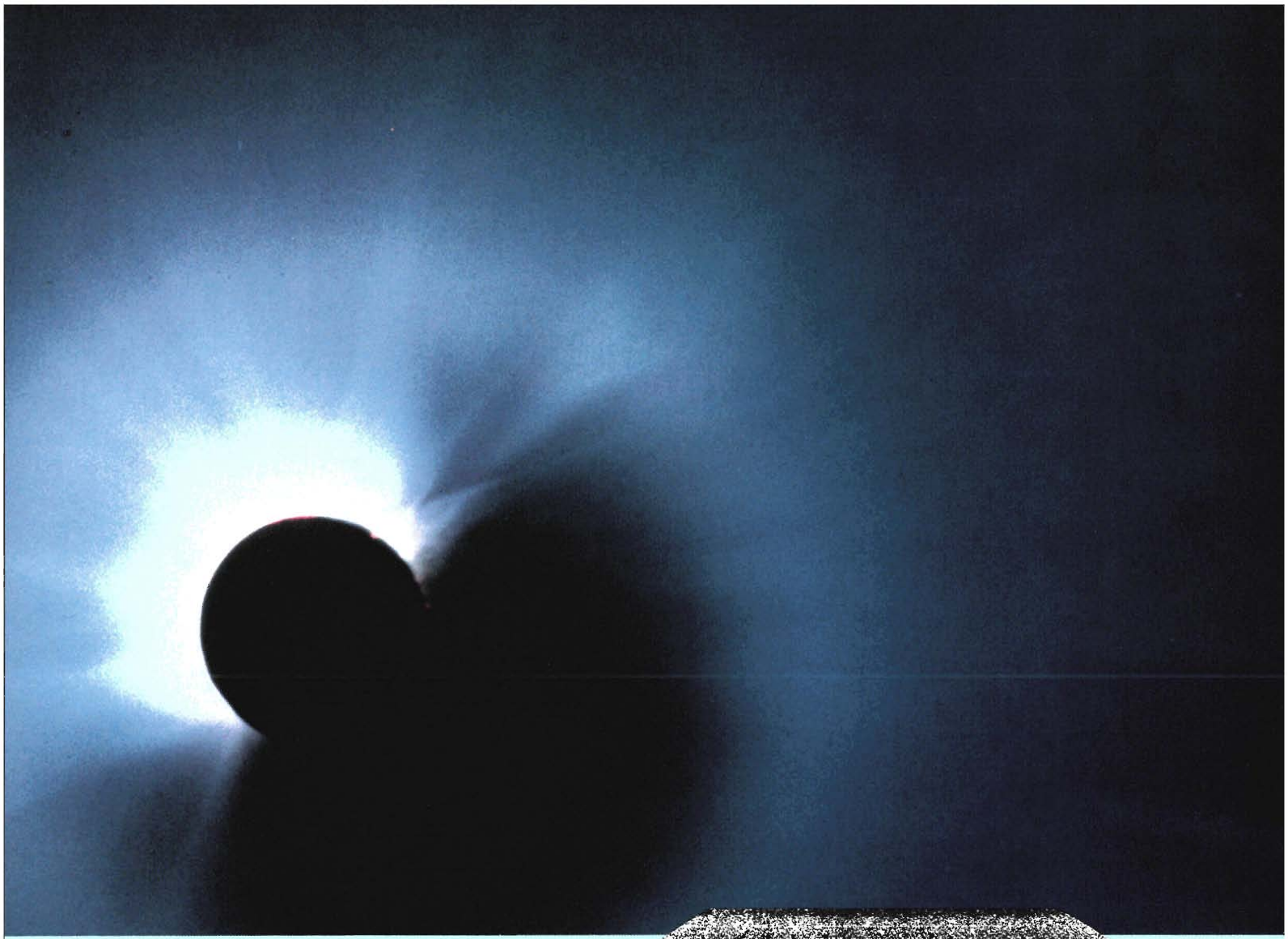

A MASS ERUPTION FROM THE SUN

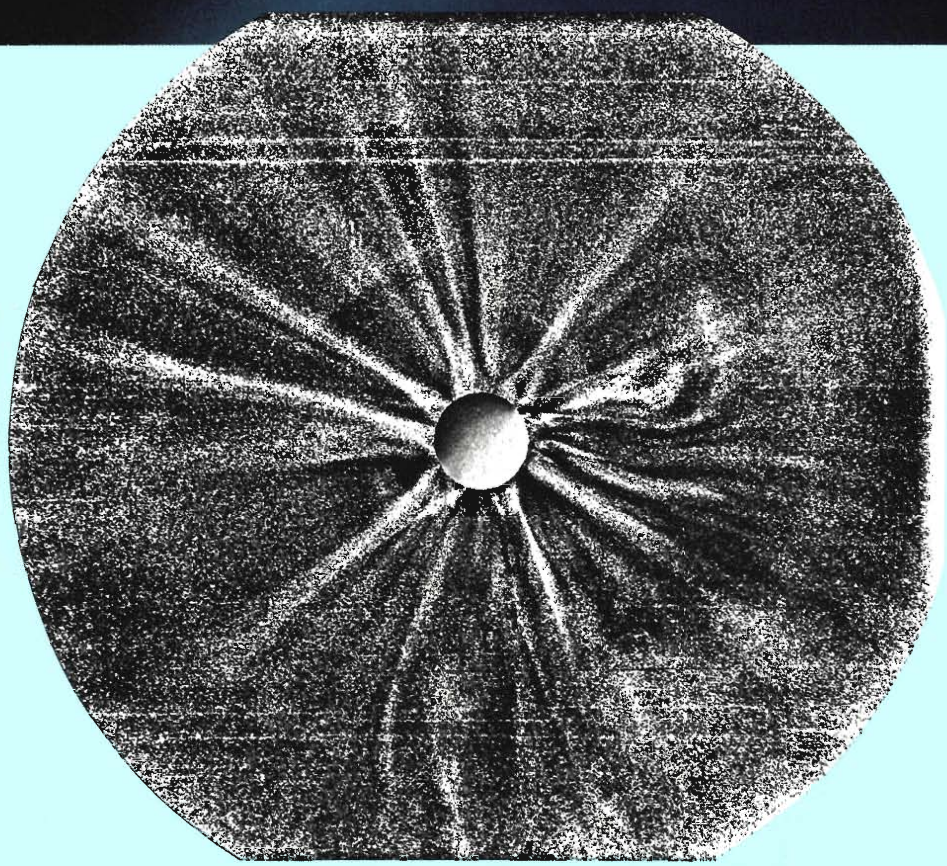

The color photograph of a huge bubble-like structure extending from the sun's limb to 7 solar radii was a most exciting result of our 1980 expedition. The structure is formed by a hydrodynamic eruptive disturbance that ejects large quantities of mass into interplanetary space. The eruption is very clearly visible on the computer-enhanced image processed from 32 digitized photographs. These large and frequent mass eruptions have been recorded since the early 1970s by Naval Research Laboratory satellites and by Skylab, but the bases of the eruptions were always obscured by the oversized occulting discs used in satellite coronagraphs. Thus ours is the first complete record of the phenomenon.

At first glance the structure looks like a tennis racket with its handle in the sun. Closer examination reveals that it is not entirely symmetric about an axis extending radially from the sun. Its polar side is markedly flattened and a density enhancement, which is possibly due to a shock wave ahead of the eruption, is very prominent above and on the equatorial side, but is nearly absent on the polar side. Nearby major streamers that usually extend in a radial direction from the sun are bent toward the disturbance, more so on the equatorial than on the polar side. In addition, the eruption may possibly be bent slightly toward the solar equator. Characteristics similar to these have been reported for eruptions observed from Skylab.

The position of this eruptive disturbance recorded from the aircraft differs markedly from that recorded by the Laboratory's rocket team in Kenya about 15 minutes earlier; from the difference we infer an expansion velocity of about 500 km/s. This value is in agreement with the eruption's absence from photographs taken from the main scientific site in India, where the eclipse occurred about 90 minutes later. During that time, the eruption would have moved beyond range of observation from the ground. If the velocity of expansion is nearly constant during its lifetime, the disturbance must have begun just as the eclipse was arriving on Africa's west coast, about 90 minutes before we saw it. We are at present trying to obtain good photographs taken from Zaire and Tanzania to study the earlier phases of the event.

Such eruptions are apparently quite common. They are estimated to have occurred at least once a day in 1973 during low solar activity and perhaps three times more frequently during this past year's maximum solar activity. Each one typically ejects a mass of about 10^{13} kg and an energy of 10^{24} J. The apparent rate of occurrence would make them responsible for at least 10% of the entire solar mass efflux!

We also obtained camera-polarimeter images and Fe XIV emission line profiles of the eruption. Its Thompson-scattered light is highly polarized so we will be able to determine electron densities and its base appears to have the most intense green line (Fe XIV) emission in the corona. We anticipate that these measurements and our photographs, which together comprise a wealth of interconnected information, will answer several questions about these important sources of solar wind ■

symmetric, this would pose no problem. But in fact its visible brightness varies markedly from one region to another. Thus interpretation of all measurements requires assumptions, based on detailed photographs, about the three-dimensional structure of the corona.

Direct Photography — Imaging the Corona

Good photographic prints of the solar corona are extremely difficult to make because coronal brightness varies by factors of 1000 from 1-4 $R_\odot$ and 10,000 from 1-10 $R_\odot$, whereas prints can display only a factor of 10. We use three methods to reduce this radial brightness gradient.

1. A radially graded filter placed just in front of the film transmits light in precisely the desired amount as a function of distance from the sun.
2. An internal occulting disc in the converging light path within the camera also uniformly reduces the brightness gradient.
3. And computer processing reduces the gradient in the digitized photographs from the electron density experiment.

All three methods were used during the 1980 expedition. Because of a slight misalignment of the mirror tracking system aboard the aircraft, the first two gave good photographic records of only two-thirds of the corona. Nevertheless these pictures give us a remarkably detailed view of the corona during the sun's maximum activity and a particularly fine look at a large mass ejection extending from the base of the corona out to 7 $R_\odot$.

One of these photographs, together

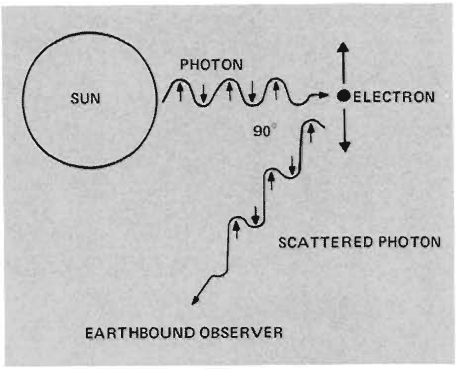

Fig. 9. Schematic of light scattered at 90° by an electron in the plane of the sky to an earthbound observer. This light is 100% linearly polarized along the direction tangent to the sun's radial vector, because its electric field vector (indicated by the arrows under the wavy lines) is always perpendicular to its direction of motion. However, not all the light we observe in our camera-polarimeter has been scattered in the plane of the sky. Each point on our digitized photograph is a sum of contributions that have been scattered from many angles into the line of sight. Consequently, the maximum observable polarization of the K corona from a spherically symmetric corona is only 67%. This theoretical maximum is reduced even further because the corona is not spherically symmetric and, in the inner corona, photospheric light is traveling in nonradial directions before being scattered. Thus the expected polarization as we move toward the sun's limb decreases from 67% to 0%.

with a computer-enhanced image processed from 32 digitized exposures taken with our camera-polarimeter, is shown in the note "A Mass Eruption From the Sun."

Electron Density Experiment

The scattering process that produces the K corona (see Figs. 6 and 7), namely, Thompson scattering of photospheric light by electrons, is independent of wavelength and depends only on electron density. K coronal intensities are thus a direct measure of electron densities. Since we can measure only total white light intensities (K + F corona), we need a method to subtract the unwanted F coronal light.

Much of the K coronal light we observe during an eclipse has been scattered through angles near 90°. The K corona is therefore highly polarized (Fig. 9), whereas the F corona is not. The two components can be separated by measuring both the absolute intensity of the K + F corona (K + F) and the fraction and direction of polarization at each point on digitized images. The measured fractional polarization can be written

$$P_{total} = \frac{P_k K}{K + F} \quad ,$$

where P_k is the fractional polarization of the K corona, and K and (K + F) are the K coronal intensity and total white light intensity, respectively. Data reduction to determine K requires a model of the corona. We assume that the corona has cylindrical symmetry and that its density varies smoothly between polar and equatorial regions. From this model, we calculate P_k and K and compare them with the measured quantities P_{total} and (K + F). Finally we vary electron densities in the model to obtain consistency between the two measured and two calculated quantities.

Photographs of the K + F corona are taken with a camera-polarimeter through plane polarizing filters oriented at three different angles. A fourth photograph taken without any polarizing filter completes a set. During the 1980 eclipse, we made 10 sets of photographs using high-resolution film for the bright inner corona and very fast low-resolution film for the outer corona. This is the first time we have taken special care to get high-resolution data from the inner corona.

The camera and its center-of-mass, three-axis gyrostabilized tracking system were designed and built at Los Alamos (Fig. 10). With this tracking system, motion during a 3-second exposure was less than 20 arc seconds. Our polarization data extend out to 12 $R_\odot$ in the equatorial region of the corona—much

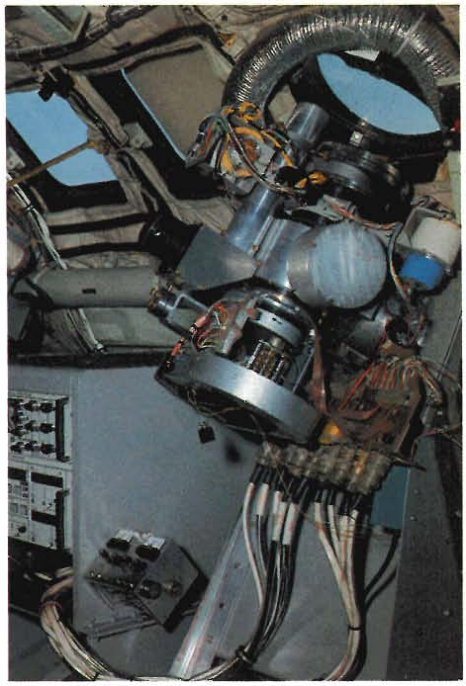

Fig. 10. Los Alamos-designed telescope for photographic polarimetry and electronic control equipment (lower left) mounted in aircraft. This instrument photographs the corona beyond 12 $R_\odot$ and has provided data for determining electron densities and image-enhanced photographs of the outer corona. (See note "Unique Record of the Changing Corona.") The blue cylinder (upper right) is one of three orthogonally mounted gyroscopes obtained from NASA's Apollo program. These provide the inertial references that allow this instrument to point at high accuracy even when the aircraft is in motion.

greater distances than have been achieved from ground observations during an eclipse or from Skylab observations outside of eclipse. In the 1979 and 1980 eclipses we were able to make two exposures out to 20 $R_\odot$.

We have made similar measurements using the same instrument at five times during the sun's 11-year magnetic activity cycle (1970, 1972, 1973, 1979, and 1980). We thus have a very uniform set of data with which to compare variations in coronal structures, brightness, electron density, and material distribution as a function of solar activity. (See note

"The Changing Corona.") For instance, standard observational models of coronal brightness indicate a marked variation between maximum and minimum solar activity. We are unique in being able to verify this variation for the inner corona (out to 3 or 4 $R_\odot$) and to extend it reliably to 12 $R_\odot$.

Results of 1973 Electron Density Experiments

In recent years the 1973 eclipse was the most widely observed both from the ground and in space. Figures 11a and b show plots of absolute intensity of the corona (K + F) as a function of radial distance in the inner and outer corona, respectively. Also included in these plots is the consensus model K + F brightness based on pre-1965 eclipse data. Figure 11a is a comparison of results from five independent observations of the 1973 eclipse: two from the ground, two from space coronagraphs, and one from the Los Alamos airborne expedition. Only the Los Alamos data extend over the entire range shown and beyond.

In comparing our results for the 1973 eclipse with those of Skylab's Apollo Telescope Mount, we were puzzled to find the Skylab values of coronal brightness disturbingly higher than ours. Upon

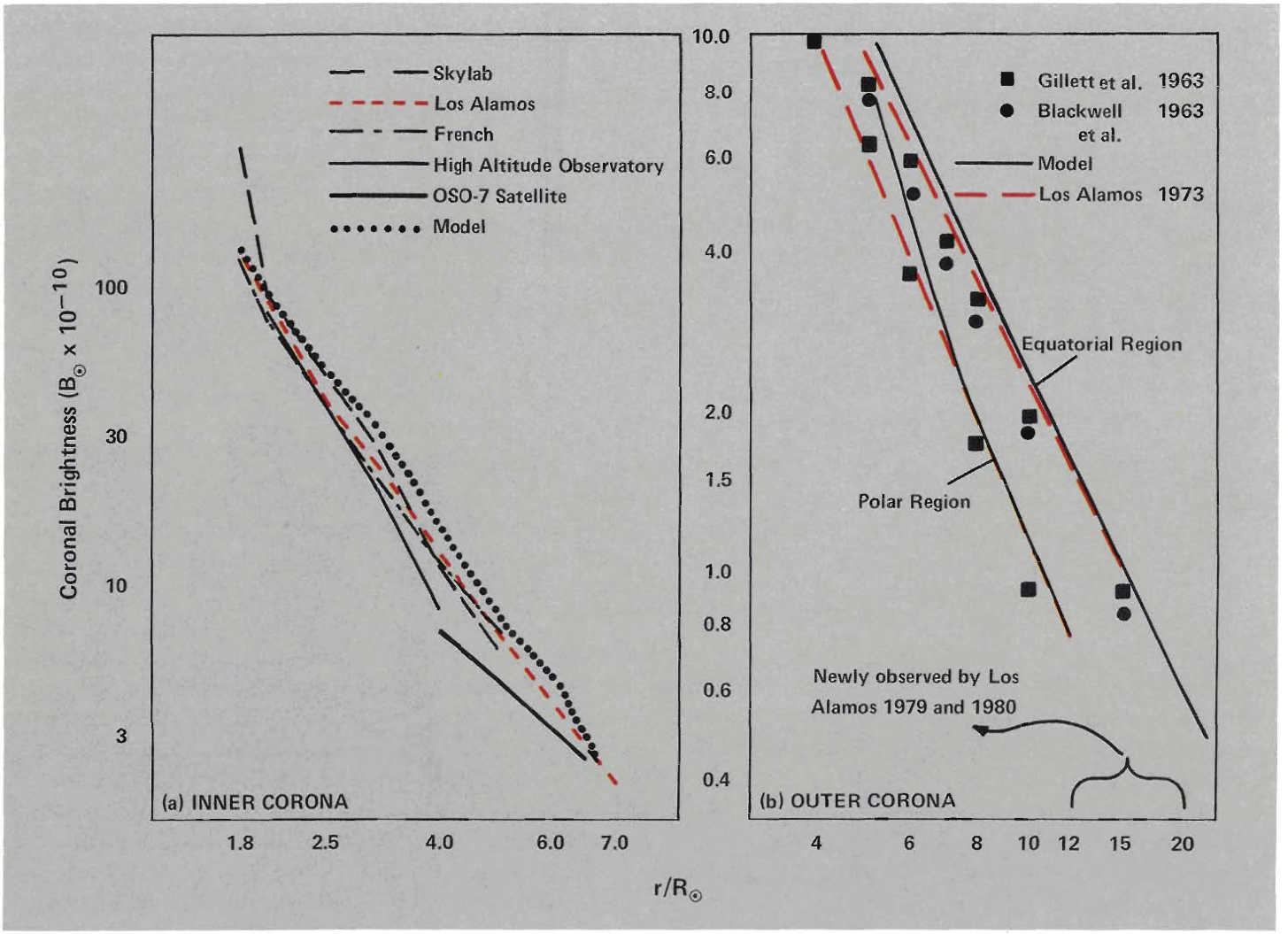

Fig. 11. Various observations of coronal brightness versus intensity for (a) the inner corona and (b) the outer corona. Also shown in both cases is the brightness calculated from a consensus model [D. Blackwell, D. Denhirst, and M. Ingham, "The Zodiacal Light," Advances in Astromony and Astrophysics , 1 (1976)]. Figure 11a is a unique comparison of cospatial, cotemperal observations from two ground-based, one airborne, and two space experiments. Only the Los Alamos data cover the entire range of comparison, and the Los Alamos 1980 data, when reduced, will extend observations to 20 $R_\odot$ for the first time since 1963.

careful examination of Skylab reduction procedure, we discovered an error in absolute calibration that resulted in a 9% reduction of all Skylab values of coronal brightness. This transfers roughly to a similar reduction in all published results prior to 1978. The intensities plotted in Fig. 11a have been corrected for this error.

Figure 11b compares Los Alamos data for the outer corona with the two best recent observations of that region.

Figure 12 shows our 1973 results compared with those from K. Saito's ground-based observations.* Because of sky background brightness, ground-based observations seldom are reliable beyond 5 $R_\odot$ in equatorial regions and 3 $R_\odot$ in polar regions, but the Los Alamos intensity data appear excellent beyond 10 $R_\odot$. Polarization measurements in the equatorial regions are also good to this distance, but over the sun's poles the K corona is so faint that polarization falls below the limit of photographic detectability at 4 $R_\odot$. We measure a fainter corona in polar regions than Saito does and therefore conclude that electron densities in polar coronal holes are lower than previously thought.

In equatorial regions the situation is more complicated. We find coronal intensity to be lower, but we measure higher polarization beyond 4 $R_\odot$. Our measurements suggest that in equatorial regions electron densities beyond 4 $R_\odot$ are higher and, more significantly for solar wind models, do not fall off as fast as we proceed outward from the sun. We also observed this significant result at the 1970 and 1972 eclipses.

We look forward to comparing electron densities from the 1973 eclipse with those of the 1980 eclipse as soon as our 1980 data have been reduced and evaluated.

Preliminary analysis of our 1980 intensity data shows that the corona was about three times brighter than it was in 1973, and that polar regions are as bright as equatorial regions out to $5_\odot$, where the F corona begins to dominate.

*K. Saito, *Annals of the Tokyo Astronomical Observatory* 13, 93 (1972).

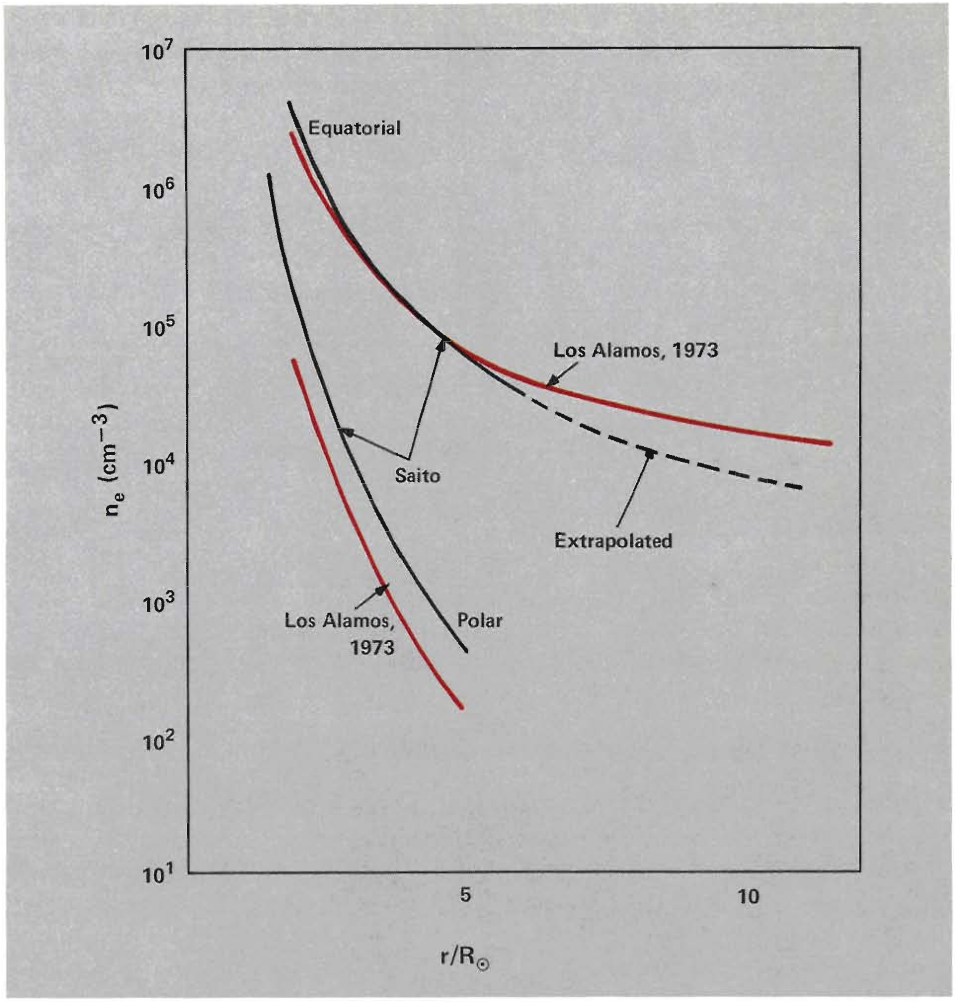

Fig. 12. Electron density as a function of radial distance determined from photographic polarization data gathered during the Los Alamos airborne expedition of 1973. The results of K. Saito, a respected ground-based observer, are shown for comparison. Photographic polarization data for the polar regions are reliable only to about 3-4 $R_\odot$, whereas absolute intensity data (see Fig. 11) are good beyond 10 $R_\odot$. We differ from Saito's results in equatorial regions beyond 4 $R_\odot$ primarily because the reduction in atmospheric contamination realized by our airborne expedition permitted us to acquire good polarization data to 12 $R_\odot$, as compared with the limit of 5 $R_\odot$ for ground-based observations.

Emission Line Experiment

We consider the coronal emission line experiment to be the most important aboard the aircraft because the measured line profiles contain a wealth of information on the state of the coronal plasma. The shape of the line profiles can be analyzed to yield ion temperatures and nonthermal components of the velocity distribution. The variations of line intensity with position, or with time, contain information about the mechanisms that excite the emitting ions. Bright features in or near the plane of the sky (plane through the sun's center perpendicular to the line of sight) easily contribute the major portion of our measured signal along a line of sight because emission line intensities fall off very rapidly with distance from the sun. Therefore we can attribute measured signals to specific coronal features with a fair degree of confidence.

Since 1965, we have made airborne measurements of the Fe XIV green line intensity and wavelength broadening using a Fabry-Perot interferometer to obtain spectral (wavelength) resolution. We chose an interferometer for several reasons. It is a relatively small instrument well suited to the space constraints

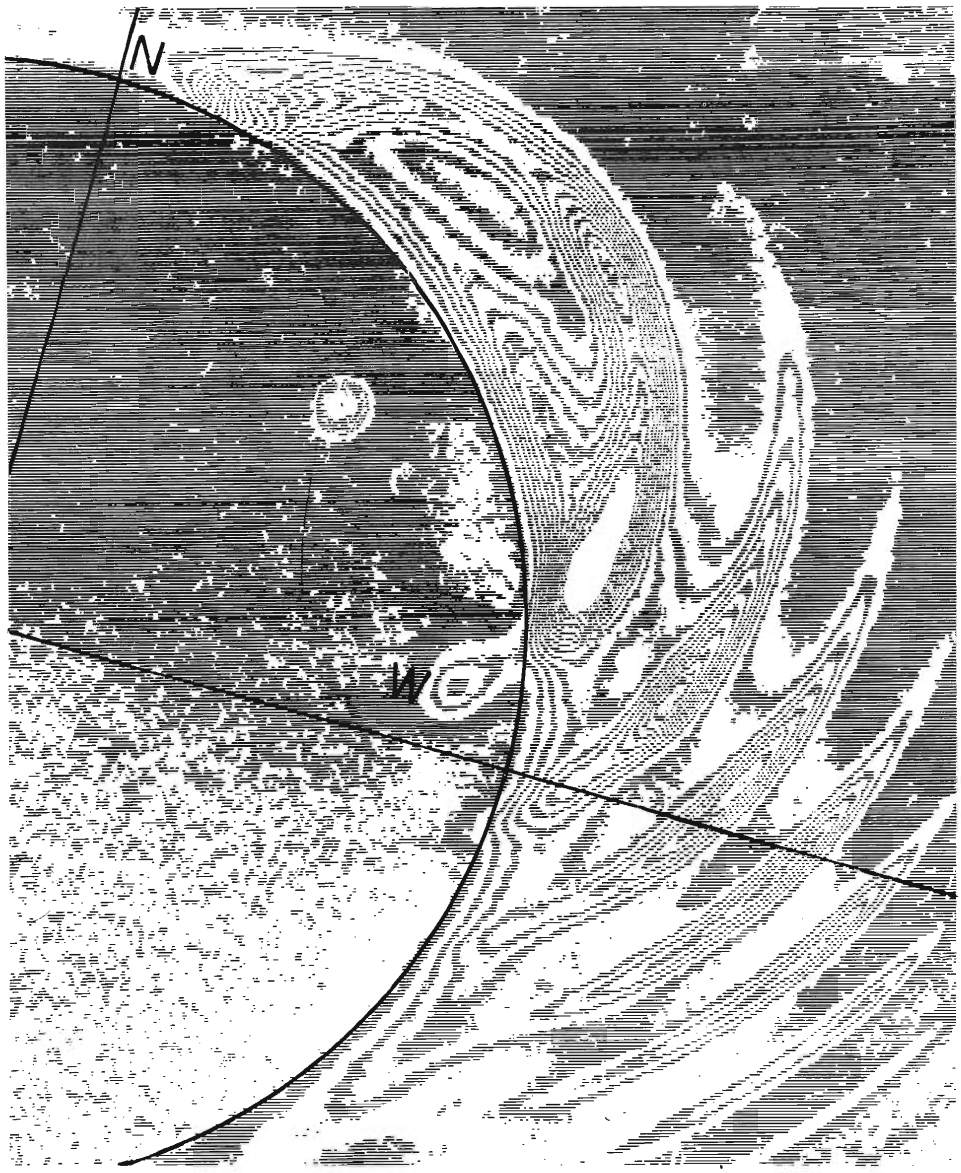

Fig. 13. Isodensity tracing of the interferometer image of the Fe XIV emission line obtained during the 1965 total solar eclipse. The heliocentric coordinates have been overlaid and the lunar limb position is indicated.

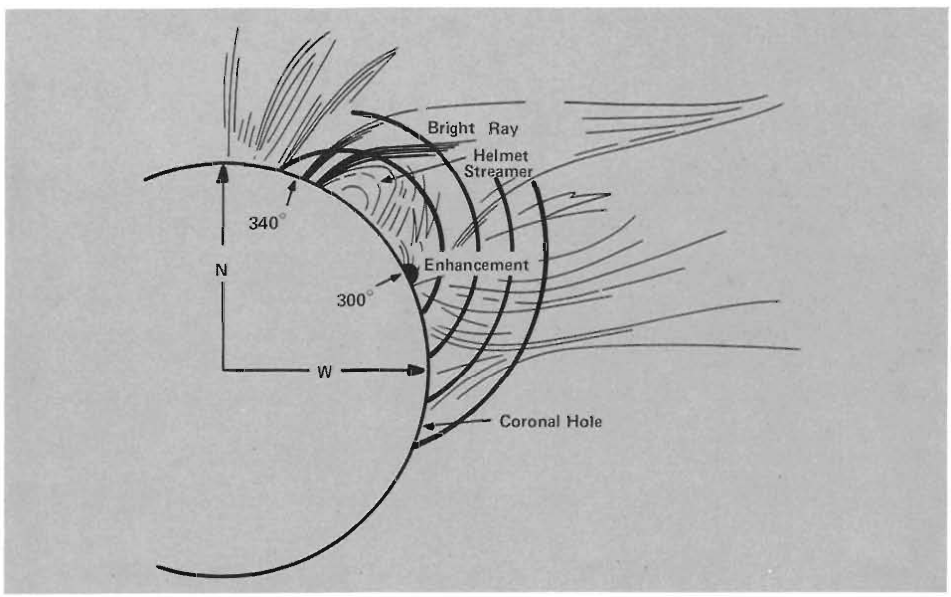

Fig. 14. An artist's sketch of the white light corona in the northwest quadrant during the May 30, 1965, total solar eclipse. The locations of the interferometer fringes are shown together with the position angles of two coronal features.

aboard the aircraft. It also has a high spatial resolution, in part because it preserves a two-dimensional image rather than the one-dimensional images obtained from grating spectrographs and other instruments that pass the incoming light through a slit. Perhaps most important, spectral distortions introduced by the interferometer can be calculated quite accurately and subtracted from the measured line profiles, enabling us to achieve very high spectral resolution.

In 1965 we obtained the first Fe XIV line profiles out to 2 $R_\odot$ from a photographic interferometer image of the corona off the sun's west limb (Fig. 13). A radial trace from the center of the fringe system through each fringe produces an intensity versus wavelength profile emitted by the corresponding region of the corona. Our spatial resolution was limited by tracking to the order of minutes of arc.

As shown in Fig. 14, these fringes passed through a helmet streamer, a coronal hole region, and an enhancement. From these data we estimated ion temperature, temperature gradients, and intensity gradients out to 2 $R_\odot$, and made the first tentative determinations of ion temperatures in helmet streamers and coronal holes at 1.5 and 2.0 $R_\odot$.

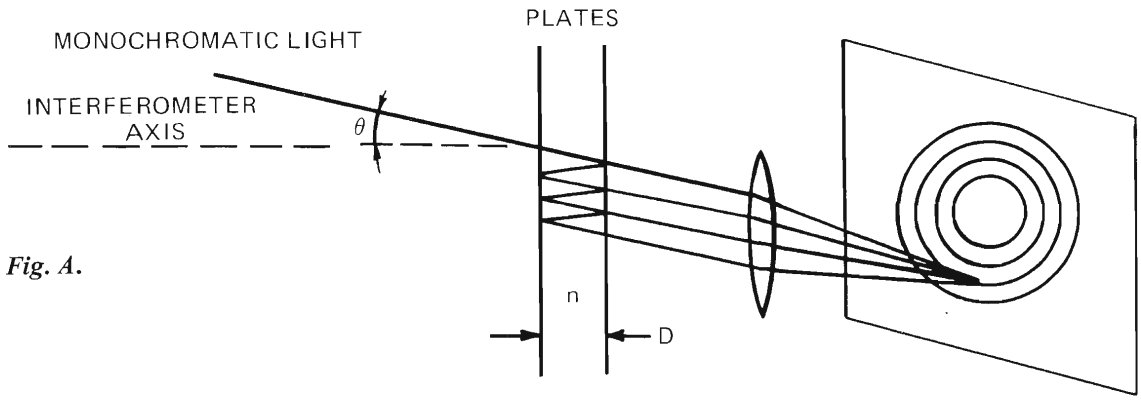

Fig. A.

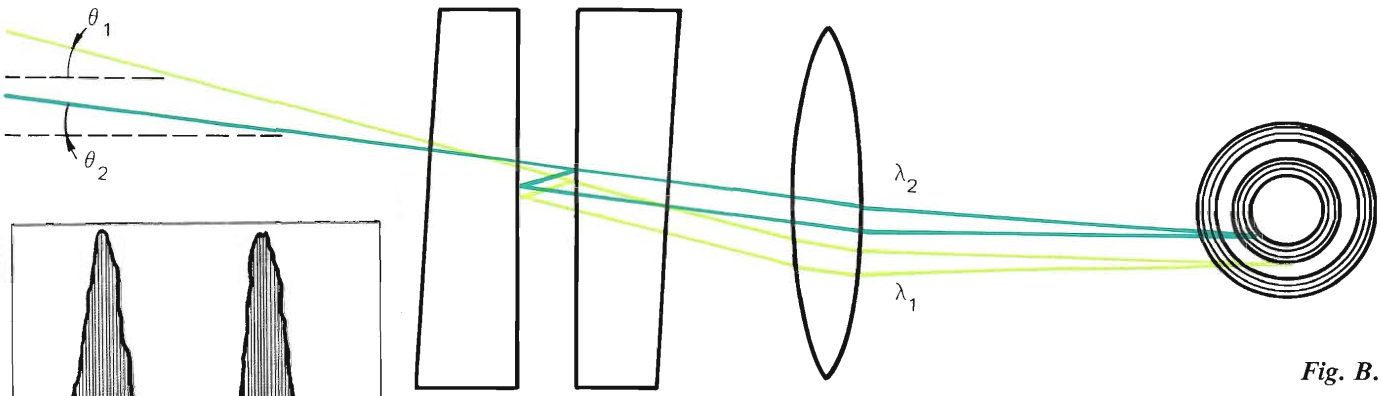

Fig. B.

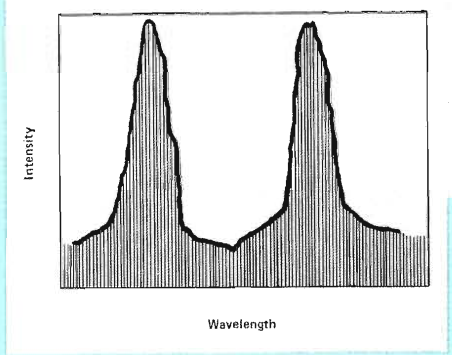

Fig. D.

THE FABRY-PEROT INTERFEROMETER

The heart of the emission line camera is a Fabry-Perot interferometer. It resolves the light from a particular atomic transition occurring in the corona into a high-resolution profile (emission line profile) of intensity versus wavelength.

The basic instrument consists of two accurately plane quartz plates maintained strictly parallel at a constant distance D. The opposing plate surfaces are coated to be highly reflecting. The plates are enclosed in an airtight chamber and the space between them is filled with gas under pressure. The index of refraction n of the gas-filled space can be varied by changing the gas pressure.

A beam of monochromatic light with wavelength λ entering the interferometer at some angle θ to its axis is reflected between the plates many times (Fig. A). The beam's optical path length is $2nD \times \cos\theta$ for a round trip between the reflecting surfaces. When this path length is exactly equal to an integral number m of wavelengths, that is, when

$$m\lambda = 2nD \cos\theta , \qquad (A)$$

then the reflected and incident light waves are exactly in phase and constructive interference (reinforcement) takes place. Successive values of m correspond to successive orders of interference. If the incident angle deviates even slightly from θ, destructive interference quickly reduces the intensity because of the large number of reflections in a highly reflective Fabry-Perot interferometer. Thus monochromatic light from an extended source produces a series of concentric bright rings corresponding to successive orders of interference.

The coronal spectrum includes many widely different wavelengths that can interfere constructively for a given value

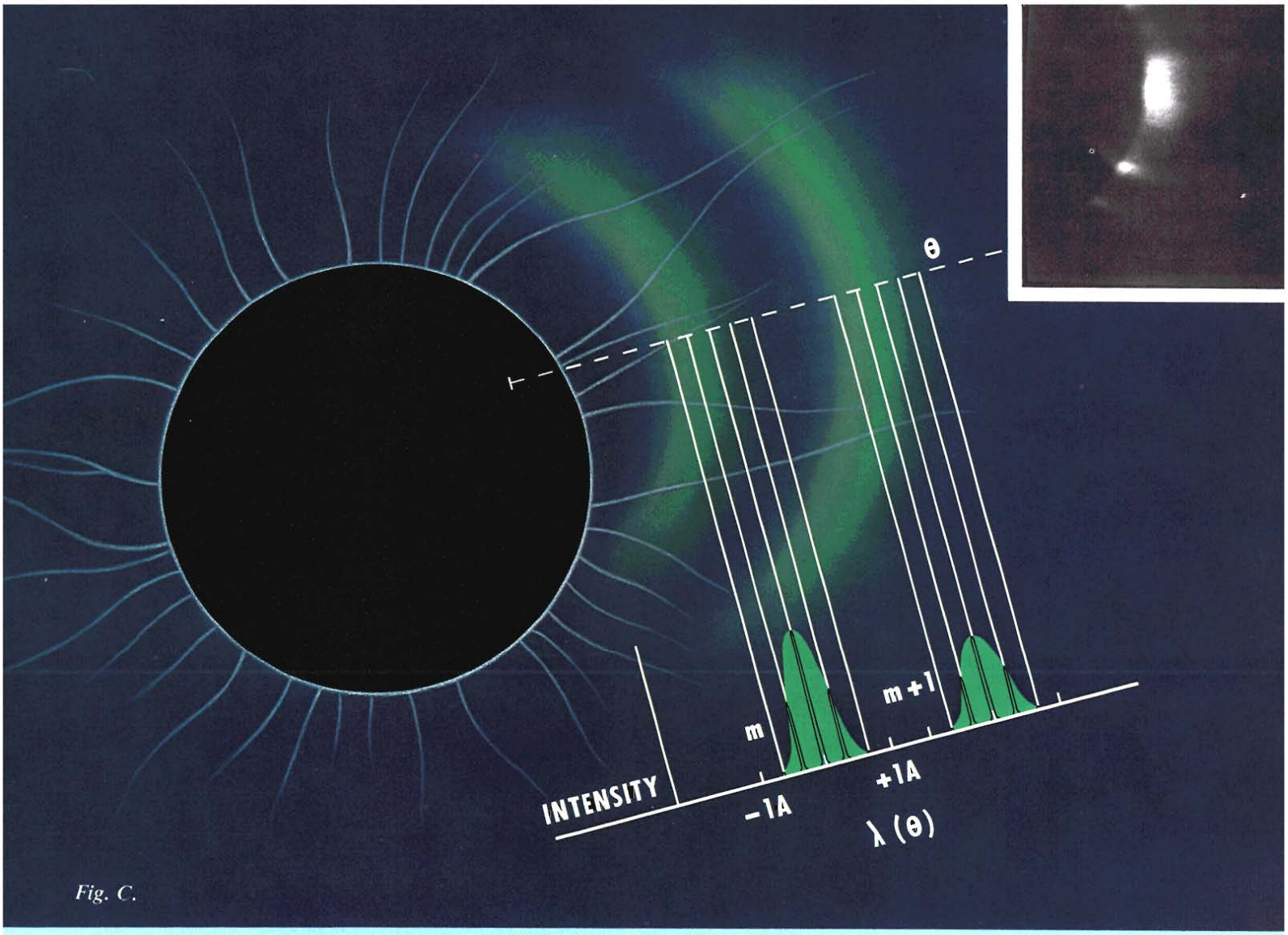

Fig. C.

of 2nD cos θ. This range is restricted by a prefilter to keep the long wavelength end of one order from overlapping the short wavelength end of the next order. The prefilter is centered on the coronal emission line being measured and transmits wavelengths over a 20 Å range.

Coronal emission lines are Doppler-broadened features roughly 1 Å in full width at half-maximum intensity. If an emission line centered at λ_1 constructively interferes for an incident angle θ_1, then another wavelength in the profile, say λ_2, entering the interferometer at a slightly different incident angle θ_2 will also interfere constructively (Fig. B). Thus successive wavelengths in the line profile are imaged by the interferometer as adjacent rings at successive values of θ, and the result is a broad ring where the profile of intensity versus λ is imaged as a profile of intensity versus θ. One carefully makes a trace radially across a ring to extract intensity versus θ, which is easily converted by using Eq. (A) to intensity versus λ (Fig. C). Note that these profiles are deduced for an extended region of the corona corresponding to less than the width of the broad interferometer rings.

The partial rings produced during the 1965 eclipse by a segment of the corona are shown in Fig. 13 of the main text. In 1965 we had time to take data only at a fixed value of 2nD, so the only regions of the corona that could be studied were those corresponding to the bright rings in Fig. 13.

During the 1980 eclipse, our rapid data-acquisition system gave us time to vary the gas pressure inside the interferometer, and thus to change n and cause the rings to traverse the entire coronal image by changing the angle for constructive interference. By thumbing the corner of this journal, on which are printed our 1980 photographs, the reader can observe the movement of the rings caused by the pressure scan. From this series of images corresponding to different values of n, we can plot the intensity change at a single spatial point as the gas pressure is varied with time. This plot of intensity versus n is converted to intensity versus λ.

Our video recording system stored an array of 250,000 spatial data points from each image; during a pressure scan of one order, 120 images were recorded. Each point can produce such a profile. One such profile is shown schematically in Fig. D. The line profile is repeated as the pressure scan moves the ring corresponding to the succeeding order across the point being plotted. The spatial resolution of a line profile deduced from a single point is 4-5 arc seconds, which is an order of magnitude better than can be obtained from a radial trace ■

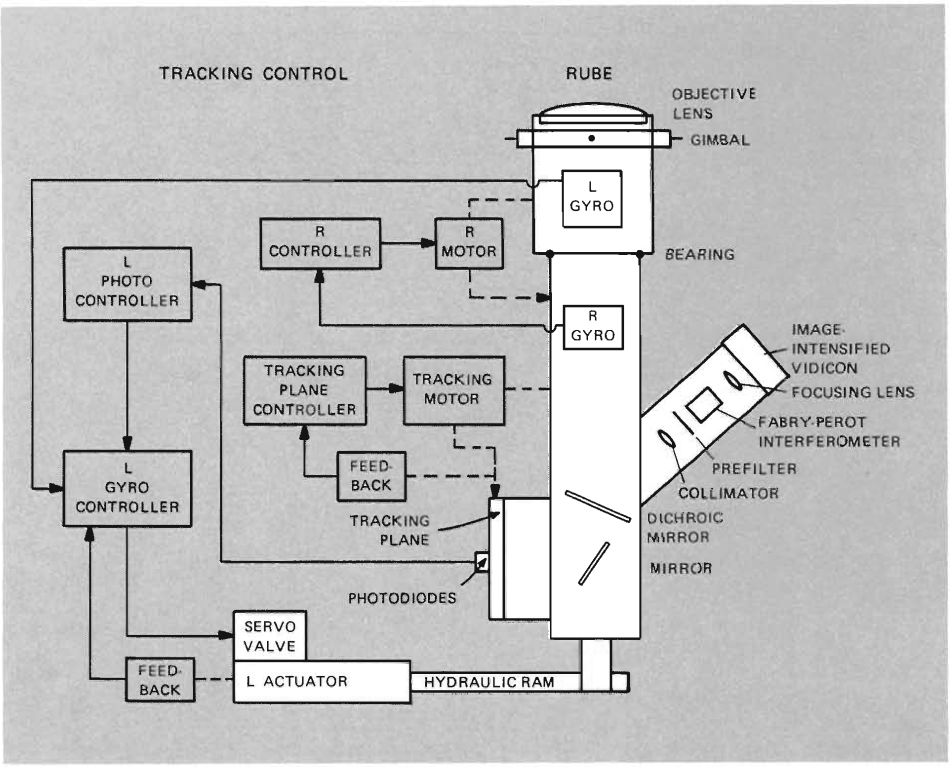

Fig. 15. Main components of the tracking control for the coronal emission line camera. Tracking along two orthogonal axes is controlled directly by an operator or by feedback from gyroscopes mounted on the telescope. Only one of these gyroscopes (L gyro) and its associated control mechanisms are shown here. Gyroscope drift in the two orthogonal axes is compensated by error signals from a set of photodiodes that views an image of the eclipsed sun. The tracking plane controller is preprogrammed with the various tracking patterns to be followed during totality. In addition, rotation of the telescope about its optic axis is required to correct not only for aircraft motion but also for the apparent rotation of the sun during the duration of totality, which amounted to nearly 2° during the 1980 eclipse. This rotation is controlled by feedback from a gyroscope (R gyro) and by preset gyroscope precession in the R controller. Error signals, the difference between a gyroscope axis and the required axis, are about 4-5 arc seconds for the telescope in flight. Similar performance accuracy has been determined from photographs and video recordings of lunar limb motion.

In 1973, we scanned the entire corona out to 2.5 $R_\odot$ with a spatial resolution of 15-20 arc seconds. We measured very weak polarization of the green line along radial vectors from the sun. Weak polarization implies that green line emission is excited by electron collisions rather than absorption of photons. This result confirms expectations that electron collisions are the dominant mechanism by which energy is distributed in the inner corona. We also observed that Ca XV yellow line emission occurred over a much larger region of the lower corona than previously expected. The presence of the yellow line was thought to signify very hot regions of the corona, corresponding to the 4-5 MK ionization potential maximum of the Ca XV ionization state, but the 1973 line widths indicate that the yellow line is produced in cooler regions as well, and thus that coronal temperatures may be much more uniform on a scale of arc minutes than had been guessed from other emission line measurements.

Our 1980 data is much more extensive and has a much higher spatial resolution than that from previous eclipses.

Light from the 1980 experiment was collected by the "Rube Goldberg," a massive 10-inch telescope with an 80-inch focal length that has been used aboard the aircraft since our 1965 expedition. Emission line signals, imaged by the telescope and interferometer, were amplified and recorded on videotape at 16-ms intervals from an image-intensified vidicon detector. This rapid data acquisition system, a dramatic improvement over the 30-second exposure times required by photographic techniques, collected well over 20,000 line profiles from the base of the corona and in some regions out to 3 $R_\odot$. The detector was designed specifically for astronomical measurements and for compatibility with standard computer image analysis equipment by M. T. Sandford. Its progenitor was developed at Los Alamos for diagnostics in the weapons program.

The line resolution and diameter of the detector, combined with the relatively large image size (we view the corona in segments), determine a spatial resolution of 4-5 arc seconds. But to realize this resolution, we must keep the image centered in the interferometer and on the axis of the telescope. We accomplish this by offsetting the entire 210-kg emission line camera (telescope, interferometer, and detector) with large hydraulic actuators that are controlled by a sophisticated tracking system accurate to 4-5 arc seconds (Fig. 15). The hydraulic actuators are able to move the massive instrument at frequencies of up to 10 Hz to correct for higher-frequency aircraft motions.

Data from the 1980 measurements are much easier to reduce than those from previous eclipses. Preliminary results show wide variations in line shapes and are suggestive of the turbulent conditions that may be present during a solar maximum. We also see many de-

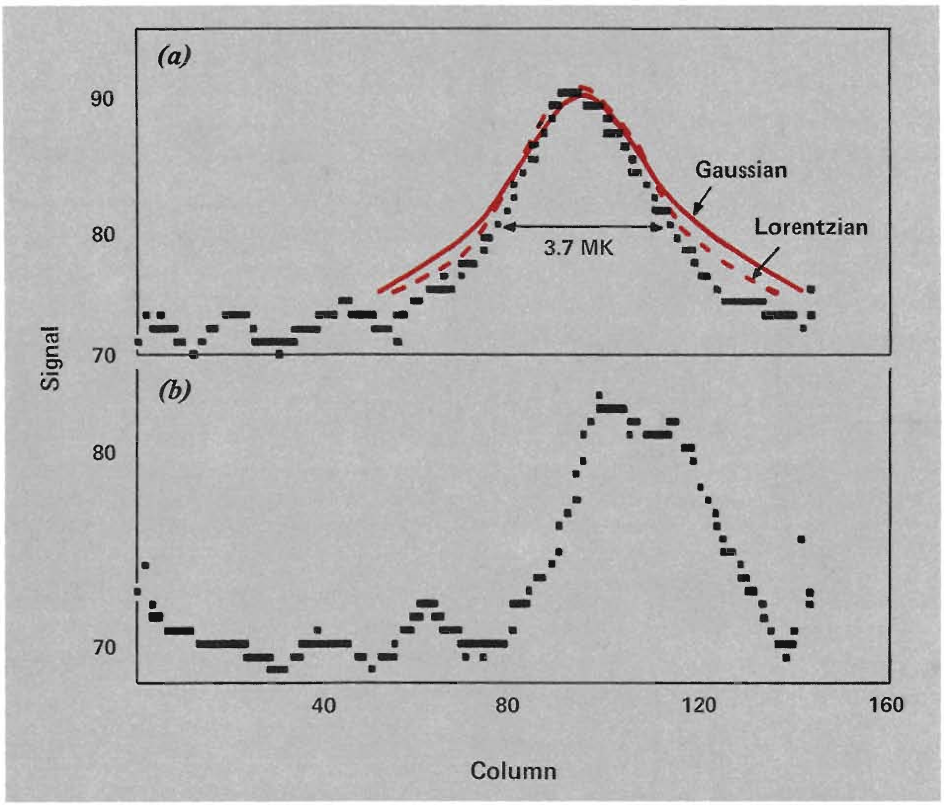

Fig. 16. These preliminary 1980 Fe XIV emission line profiles were obtained by digitizing a sequence of video frames and reordering the data to give a signal versus frame number (or wavelength) profile of the intensity at a single pixel (corresponding to a single spatial location in the corona). In (a) we have fitted both a Gaussian and a Lorentzian profile to the emission line such that the full width at half-maximum intensity and the peak intensity agree with observations. The wings of the observed line are not fitted by either profile. In (b) an example of a more complicated emission line is shown. This profile could represent coronal material with significantly different velocities along the line of sight. A relative velocity of about 15 km/s would fit this profile. Some further corrections for intensity and wavelength calibration will be applied to these data before our analysis is complete.

tails within small regions of high activity. However, data reduction must be completed before we can make definitive interpretations.

Interpreting Emission Line Profiles

Both line shapes and line intensities are analyzed to learn about the conditions in the coronal plasma. Since the intrinsic line widths (from ions at rest) are extremely narrow, the observed Doppler-broadened line profiles are identical in shape to the velocity distribution of the emitting ions.

For ions in thermal equilibrium, both the velocity distribution and the emission line profile would be Gaussian in shape. The width of the line profile would then be proportional to the kinetic temperature of the emitting ions. However, ion temperatures deduced directly from observed Gaussian line profiles (for example, the iron temperatures shown in Fig. 5) may be too high because nonthermal effects, such as macroscopic turbulence and magnetic wave acceleration of the solar wind, may add to the velocities of the ions and, in turn, to the line broadening.

An approximate expression for the line width in terms of the kinetic temperature T and the average turbulent macroscopic velocity v_t is given by

$$\frac{\Delta\lambda}{\lambda} \propto \left(\frac{T}{m} + v_t^2\right)^{1/2} ,$$

where $\Delta\lambda$ is the full width of the line profile at half-maximum intensity and m is the mass of the emitting ion. Note that the kinetic temperature contribution depends on the mass of the ion, whereas the contribution from macroscopic turbulence is mass independent. Therefore it is possible to separate thermal and turbulent contributions to the line broadening by measuring emission line profiles of two ions with widely differing masses. But these measurements must be made at the same time and at the same place in the corona so that we can assume that the two ions have the same kinetic temperature and average turbulent velocity v_t.

Our Ca XV data from the 1980 eclipse may be appropriate for comparison with our Fe XIV measurements, but the emission was weaker than expected and so the profiles may not be accurate enough. However, the Lyman-α data recorded by rocket experiments at several places in the corona will certainly be useful in determining nonthermal contributions to our Fe XIV line profiles.

Variations in line shape are also indications of nonthermal velocities. For example, calculations show that large expansion velocities from solar wind flow tend to flatten and extend what would have been a Gaussian line shape. Although these departures are not significant until expansion velocities are 40 km/s or greater, such velocities are predicted by some models of solar wind flow at distances of 2-3 $R_\odot$. The line profile shapes are also altered by large-scale turbulent motion or significant magnetic wave acceleration of the plasma.

Figure 16 illustrates the variety of line shapes that were actually measured in 1980. We see asymmetries, as well as departures from Gaussian shapes. In-

terpretation of these line shapes depends on theoretical assumptions and supporting data, except perhaps for the case of split lines, which clearly indicate relative bulk motion of the emitting material.

Analysis of line intensities can also be quite revealing. Since emission intensity depends on density and temperature, comparison with independent electron density measurements is helpful in deciding whether bright regions are due to high temperatures or, alternatively, to high densities. We can also analyze intensity variations as a function of radial distance to infer excitation mechanisms. If ions are excited by electron collisions, intensities are proportional to the square of the electron density $(n_e)^2$ and thus should decrease as $1/r^{12}$. On the other hand if photon excitation is the dominant mechanism, then line intensities are proportional to n_e and thus decrease as $1/r^6$.

Finally we can try to find periodic variations in intensity and line shape to identify wave heating of the corona. We have recorded tentative evidence of periodic variations in some of our 1973 data taken aboard the Concorde during a record-setting 74 minutes of totality (Fig. 17).

Emission Line Data Results and Questions

Our 1965 results (see Fig. 5 for average ion temperature values) showed ion temperatures decreasing outward from the base of the corona with little variation in temperature from one coronal feature to another. A more detailed look at the data in each feature is illuminating.

HELMET STREAMER. One interferometer fringe (see Figs. 13 and 14) crossed a helmet streamer near the top of the helmet at 1.4 $R_\odot$ where field lines begin to change from a closed loop to an open-line configuration extending radially from the sun. Since particles in the helmet are presumably trapped along magnetic field lines, the helmet should have above-average temperatures. In particular, along a line through the top of the helmet we should see a temperature increase in the helmet and a temperature decrease on either side. However, our 1965 data (Fig. 18) show that temperatures along this line fluc-

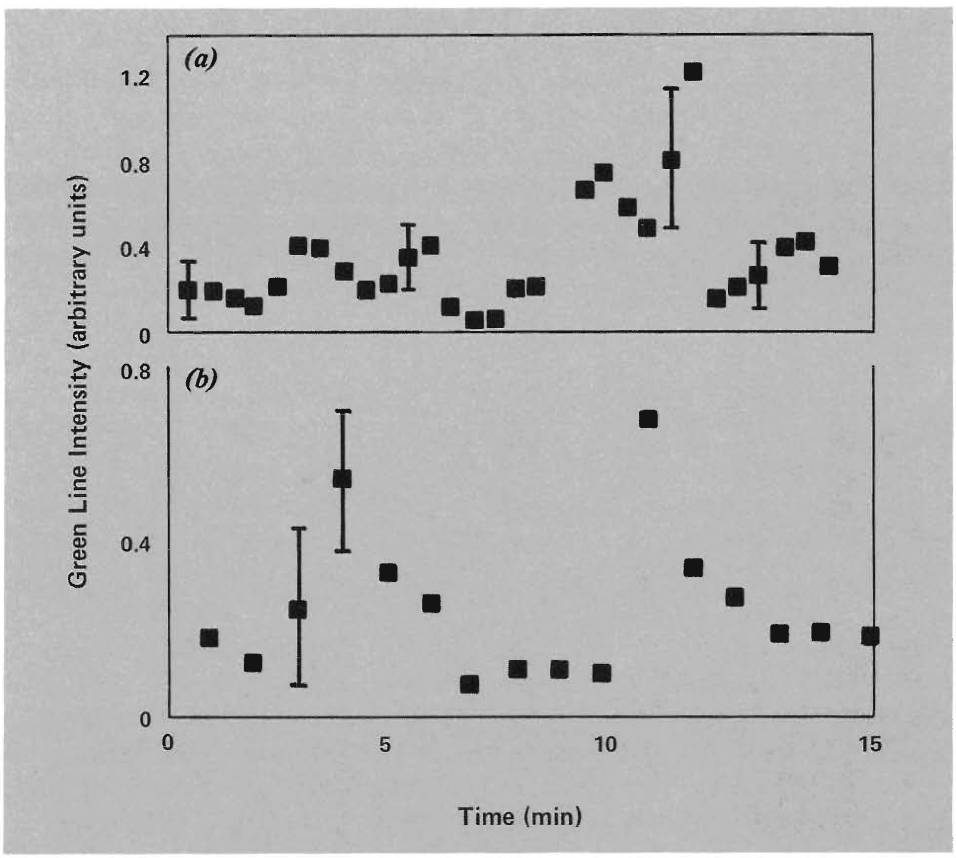

Fig. 17. Peak intensity versus time for two 15-minute segments of Fe XIV emission line data obtained aboard the Concorde 001 at the June 30, 1973, total eclipse. The data in (a), from a region near the base of a helmet streamer at 1.07 $R_\odot$, suggest intensity variations with a periodicity of about 5 minutes corresponding perhaps to a coronal response to the 5-minute oscillations of the photosphere. Tracking problems introduced the errors shown by the bars. The data in (b) are from an equatorial bright coronal region at 1.07 $R_\odot$. The sudden intensity increase followed by a slow decay suggests the presence of a shock disturbance. The variations have a periodicity of about 6 minutes.

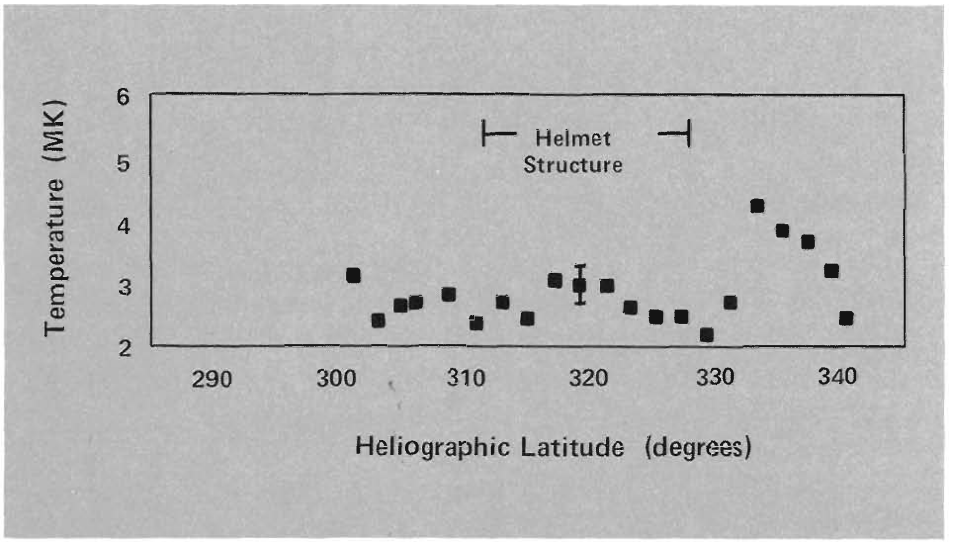

Fig. 18. Temperatures across a helmet structure deduced from Fe XIV emission line data obtained during the May 30, 1965, total solar eclipse.

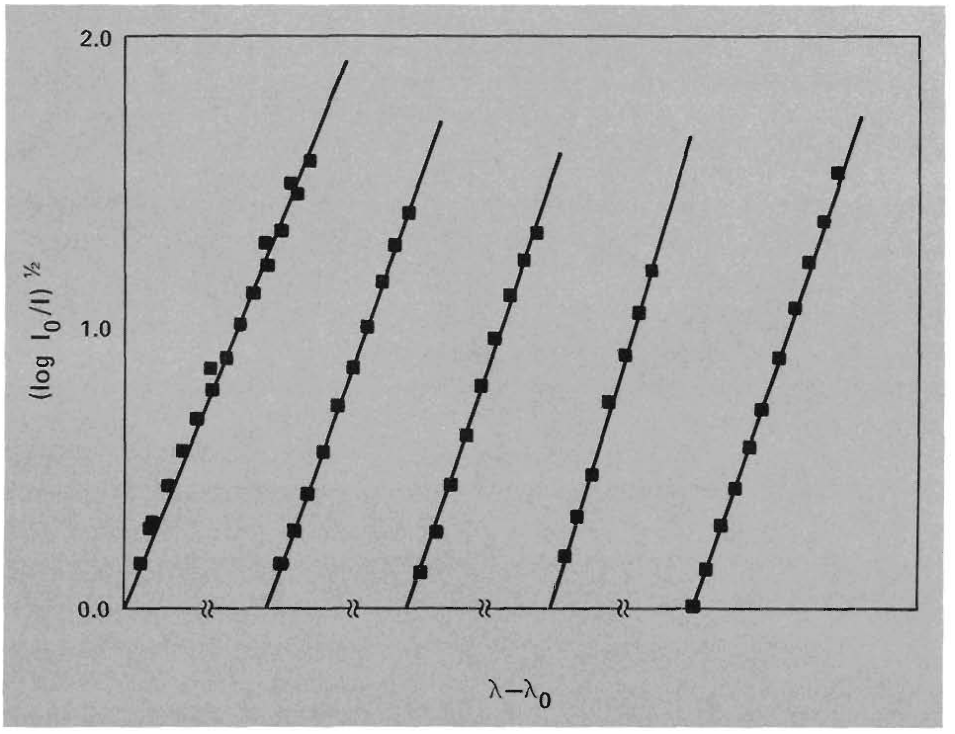

Fig. 19. Intensity versus wavelength profile of the coronal Fe XIV emission line obtained during the May 30, 1965, total solar eclipse. The maximum intensity I_0 is at the central wavelength λ_0. A straight line fit indicates a Gaussian line shape.

tuate from about 2.5-3.0 MK without much systematic change. The Gaussian line shapes from the helmet (Fig. 19) suggest that, as expected, turbulent velocities are small, perhaps less than 25 km/s in this long-lived magnetically confined region.

Our 1980 data will provide a more detailed look at the temperature structure across a helmet and will extend our view of the region above the helmet where the field lines open to form a streamer. We are particularly interested in knowing whether temperature gradients above the helmet are consistent with solar wind flow. At present the contribution of streamer regions to the solar wind is poorly known.

CORONAL HOLES. Several fringes of our 1965 data crossed a coronal hole region, so we were able to estimate temperature gradients as well as temperatures in this region. Coronal holes are expected to have lower temperatures and densities than other regions, and since they are known to be a source of solar wind flow, we expect temperature gradients consistent with solar wind theory.

One surprise was the high temperatures (2.0-2.5 MK) out to 1.7 $R_\odot$, much higher than those determined for the base of the coronal holes by the EUV measurements.

Our temperatures, which we estimated directly from line broadening, would be slightly less but still much higher than those determined from other experiments, if turbulent velocities contribute to the line broadening. In fact, we have invoked turbulent velocities in some parts of this region to deduce temperature gradients consistent with solar wind flow. If the temperature at the lowest observed altitude (1.42 $R_\odot$) is fixed at 2.5 MK, then successive temperatures at 1.62 $R_\odot$ and 1.74 $R_\odot$ are 2.43 MK and 2.39 MK, respectively, provided the turbulent velocities at these three altitudes are 35, 10, and 5 km/s, respectively. The temperature variation is then $T \propto (1/r)^{0.5}$.

We also determined the variation of line intensity with radius in this coronal hole region. Figure 20 shows that intensities fluctuate rapidly near the base of the corona, but at greater heights the intensity is proportional to $1/r^{12}$, or $(n_e)^2$. This rapid falloff is consistent with a collisional excitation mechanism—a rather surprising result given the very low density in this region determined by independent electron density measurements. However, if magnetic field lines are clustered, rather than uniformly dis-

tributed, and if electrons are trapped along these clustered lines, then the average electron density would remain low, as measured along a line of sight, but local densities would be high enough to produce ion excitations by collisional processes. Evidence for density inhomogeneities is seen on white light photographs of the corona, but whether these inhomogeneities correspond to clustering of field lines is not at all certain. More detailed intensity measurements from the 1980 eclipse may clarify the situation.

CORONAL ENHANCEMENT. A coronal enhancement is a long-lived region of higher density that overlies an active region in the photosphere. Consequently, we expect higher turbulent velocities in such a region than in helmet streamers. From our 1965 data we estimated temperatures of ~3.0 MK after subtracting turbulent velocity contributions to the broadening. Turbulent velocities in the enhancement are about 25 km/s and decrease with altitude. Temperature gradients, when corrected for turbulent velocity broadening, suggest that solar wind flow is probably very weak in this region.

We also determined intensity variation with radial distance from 1.1 to 1.6 $R_\odot$. Electron density decreases by a factor of 10 over this region. As seen in Fig. 20 intensity falls off as $1/r^{12}$ or as $(n_e)^2$; collisional excitation, as expected, dominates in this relatively dense region.

THE 1980 CONDENSATION. One of the most exciting observations during the 1980 eclipse was the hydrodynamic eruptive disturbance from the base of the west limb of the sun out to 7 $R_\odot$. From a first look at our Fe XIV emission line data we have been able to identify a very

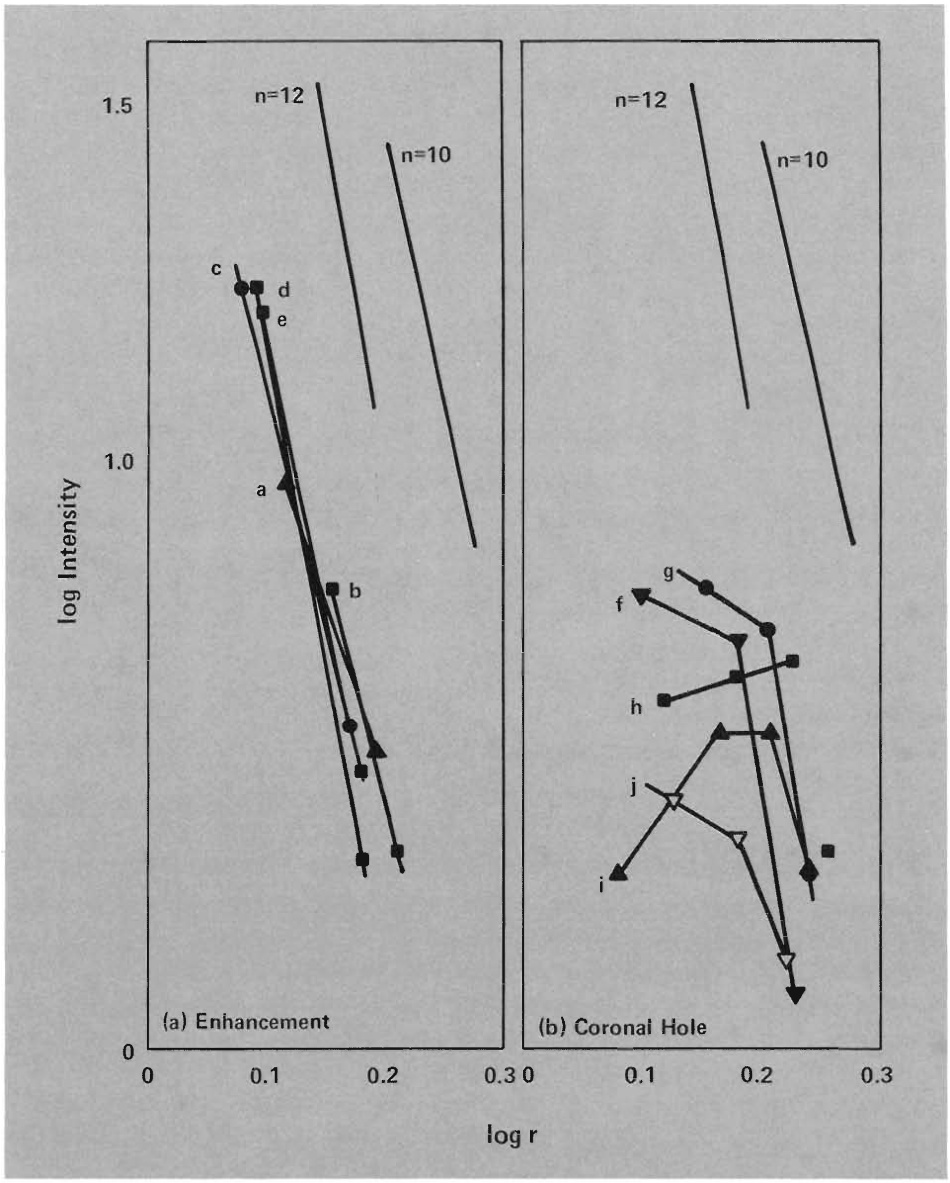

Fig. 20. Emission line intensity versus radial distance for (a) a coronal enhancement and (b) a coronal hole region. Data were obtained during the May 30, 1965, total solar eclipse. Letters label lines through data taken at the same position angle. Curves of $1/r^n$ ($n = 10$ and 12) are shown for comparison.

bright region on the west limb (Fig. 21) whose position angle is near that determined for the eruptive disturbance photographed by the coronal camera. We recorded this region a second time when we were looking for the Ca XV yellow line. The bright knot appears again, this time in the K coronal light from Thompson scattering that is accepted by the interferometer along with the yellow line (Fig. 22). The K coronal brightness in this region indicates high electron densities and so the Fe XIV brightness is probably related to increased density and not just to a temperature close to the Fe XIV ion population maximum. This region has the right size and density enhancement to qualify as a coronal condensation. If other observations taken a day or two later show that this condensation is sporadic or short-lived, we might speculate that perhaps many such condensations are related to the development of hydrodynamic eruptive disturbances. Then previous observations of coronal condensations might be used to determine the frequency of such mass eruptions throughout the solar activity cycle.

NEW CORONAL IMAGING TECHNIQUE. The emission line data from the

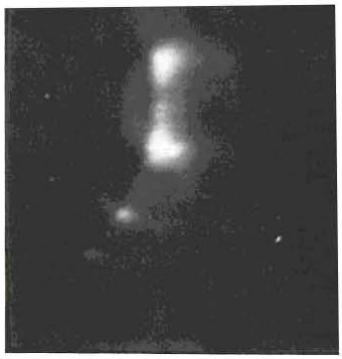

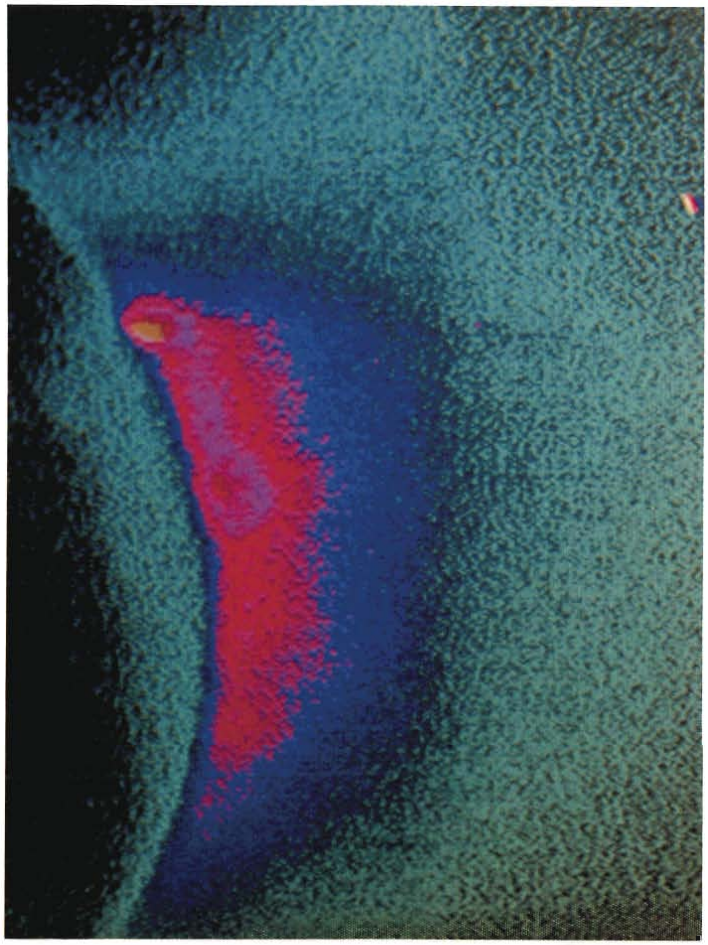

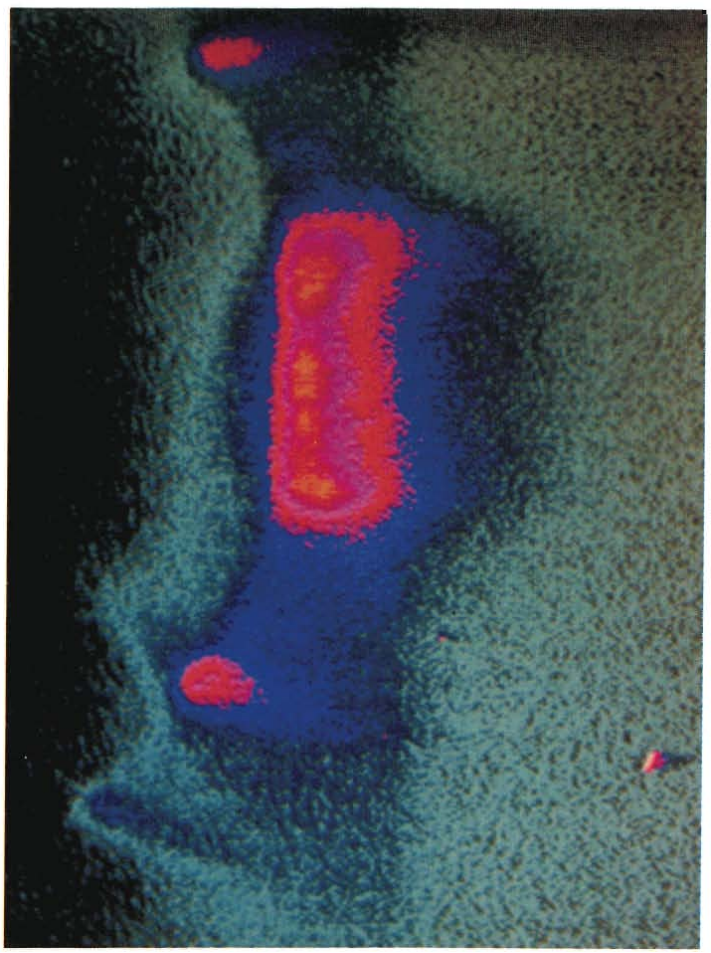

Fig. 21. False colors in this photograph of the Fe XIV emission represent intensity levels, yellow being the most intense. The central fringe was stopped near the west limb. Spatial variations in the emission line intensity are fine scale and regions 20 arc seconds (4 × 4 pixels) in area are observed at various position angles. Data were obtained during the February 16, 1980 total eclipse.

Fig. 22. Intensities of the Ca XV emission line are shown here in false colors, but with enough amplification to bring out the electron-scattered K coronal light. The bright knot is a high-density region and would explain the intense Fe XIV line emission from this same position angle. If the umbilical connection with the hydrodynamic eruptive disturbance (observed in K corona light) is extended back to the solar surface, this bright knot has a corresponding position angle. Data were obtained during the February 16, 1980 total eclipse.

scanning interferometer can be used to obtain a picture of the corona in the light of an emission line. Although such photographs have been obtained with expensive Lyot filters specially designed for operation at one wavelength, the new technique we present here is cheaper and quite adaptable to a variety of wavelengths. A pressure scan over one order of the interferometer is integrated onto a single photograph. As shown in Fig. 23, details of the base of two helmet streamers, the bright knot, and other features on the west limb can be seen on such an image.

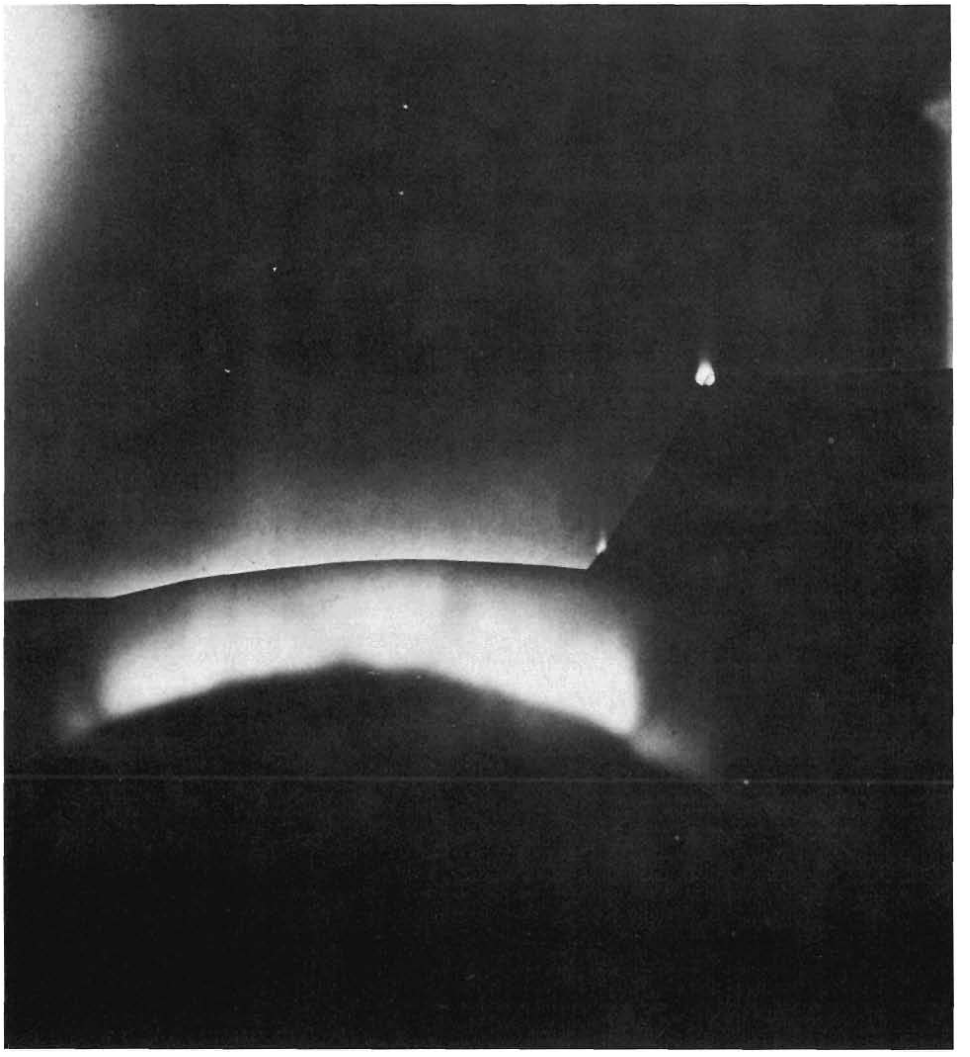

Fig. 23. Photograph of the green line corona off the west limb. This image was processed from a pressure scan of one interferometer fringe. Visible features include two helmet streamers and a bright knot.

Electron Temperature Experiment

Coronal electron temperatures as a function of radial distance are badly needed to determine whether electrons and ions are in thermal equilibrium. In 1976 L. E. Cram* suggested a method to determine these temperatures from spectral intensities of the K corona. Our 1980 attempt to perform the measurement used a much more sensitive technique than has been tried before and, although we failed to record data, we did confirm the feasibility of the technique.

The principle behind the experiment is based on Cram's analysis of the K coronal spectrum. This spectrum is formed as light coming from the photosphere (the Fraunhofer spectrum) is scattered by energetic coronal electrons. The Doppler shifts suffered by these scattered photons broaden the absorption lines in the original Fraunhofer spectrum to produce the diffuse spectrum known as the K corona.

Cram's calculated spectra for a spherically symmetric, isothermal corona at four electron temperatures are shown in Fig. 24. His results display two very interesting features. First, there exist spectral "nodes," that is, wavelengths at which the intensity is independent of the assumed electron temperature. These nodes occur on either side of the H and K absorption lines of Ca II and near other absorption features of the Fraunhofer spectrum. Second, the spectra undulate about these nodes with an amplitude that is related to the electron temperature. Thus, the ratio of two measured intensities, one at a nodal wavelength and one at a wavelength nearby, should determine the electron temperature uniquely.

Although such an experiment is very simple in principle, in practice it is quite difficult because the intensities must be measured with great precision. An error of $\pm 0.2\%$ in the intensity ratio translates to an uncertainty of ± 0.1 MK in coronal electron temperature. The 5-10% errors common in standard photometric techniques would obliterate the information sought (as learned by Menzel and Pasachoff* who searched without success for residual depressions from the H and K absorption lines of CA II in photographic records of absorption spectra from the 1936 total eclipse).

To achieve the required sensitivity, we built our instrument around the only type of detector suitable for the task—an array of silicon photodiodes. These solid-state photosensitive devices have very high quantum efficiency in the spectral range of interest.

A commercially available detector, consisting of a linear array of 512 silicon photodiodes on a single integrated circuit, served as the main component of our K corona spectrograph (Fig. 25). This large array enabled us to look not just at two wavelengths but at

L. E. Cram, "Determination of the Temperature of the Solar Corona From the Spectrum of the Electron-Scattering Continuum," Solar Physics **48**, *3-19 (1976).*

D. H. Menzel and J. M. Pasachoff, "On the Obliteration of Strong Fraunhofer Lines by Electron Scattering in the Solar Corona," Publications of the Astronomical Society of the Pacific **80**, *458 (1968).*

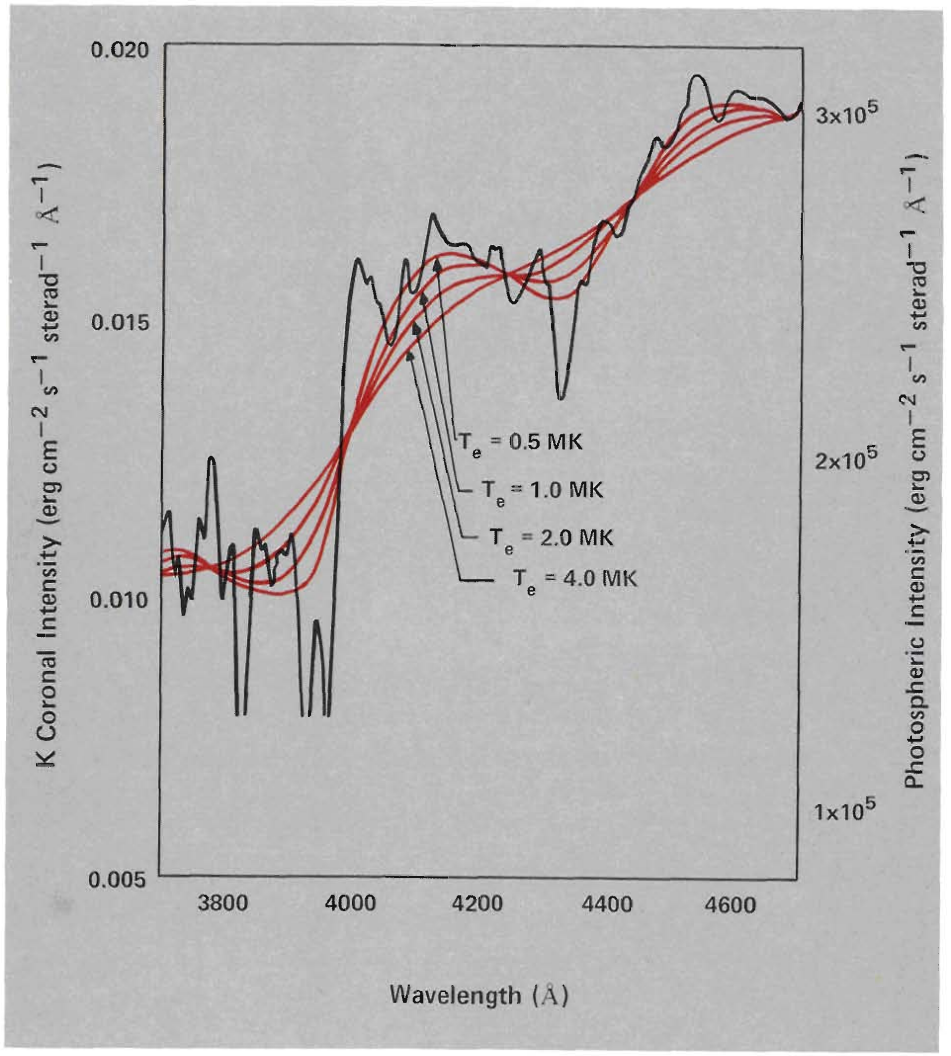

Fig. 24. Absolute intensity of the K coronal spectrum for four coronal electron temperatures, as calculated by Cram. The absolute intensity of the photospheric spectrum from the center of the sun's disc is shown for comparison.

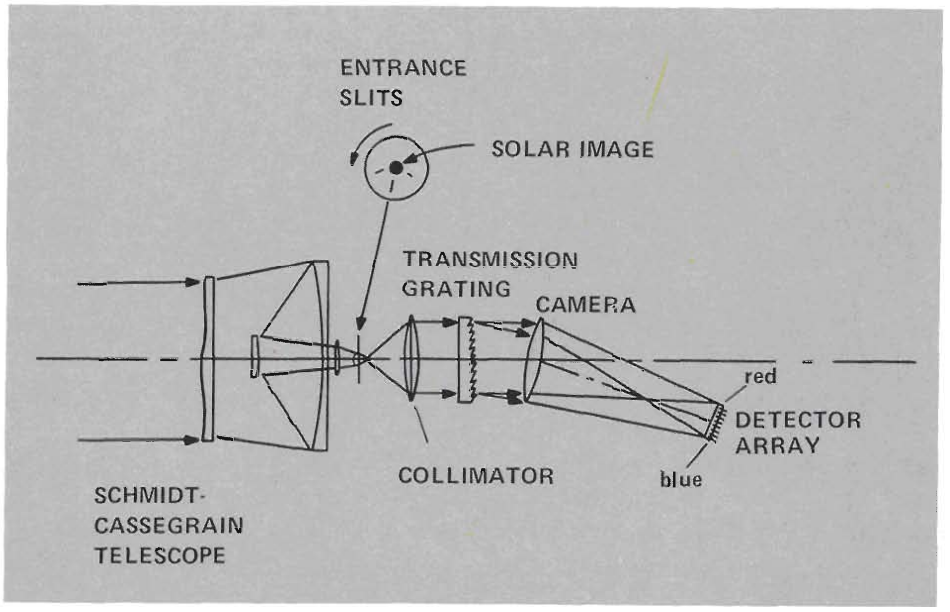

Fig. 25. The K corona spectrograph for the electron temperature experiment consists of a telescope, entrance slit assembly, a transmission grating spectrograph, a silicon photodiode detector array, and electronics for data acquisition and storage. The f/2.0, 400-mm focal length telescope maximizes the light at the detector. Three entrance slits, corresponding to radial distances from the sun of 1.2, 1.6, and 2.0 $R_\odot$, were formed by photolithographic techniques on a glass disc. A computer-controlled lever-arm and motor-drive assembly positions the selected entrance slit in the telescope focal plane. The entrance slit length is magnified by the spectrograph to match and thereby utilize the entire photodiode length. The spectrograph covers 1500 Å and its resolution is 3 Å per channel. Exposure times range from 10 seconds at 1.2 $R_\odot$ to 40 seconds at 2.0 $R_\odot$. Satisfactory data can therefore be obtained only during eclipses of relatively long duration or from aircraft whose flight path lengthens the duration of totality.

wavelengths of the K coronal spectrum over a 1500 Å range with 3 Å resolution.

The experiment was in some sense a fishing expedition. We set out to observe the entire spectrum with high precision and search for Cram's predicted undulation patterns at three radial distances from the sun.

During the eclipse, the spectrograph appeared to function well, and we were able to confirm that its sensitivity is adequate to measure the shape of the K coronal spectrum and, in principle, to determine electron temperatures. The data that appeared on our monitoring screen were not recorded by our computerized data-acquisition system (Fig. 26) because both the computer disk drive and the back-up drive failed to function.

Indeed the equipment failure was a tremendous disappointment, but we did prove that the experiment was feasible, and are now redesigning some of the electronics with hopes of flying again during the 1983 solar eclipse.

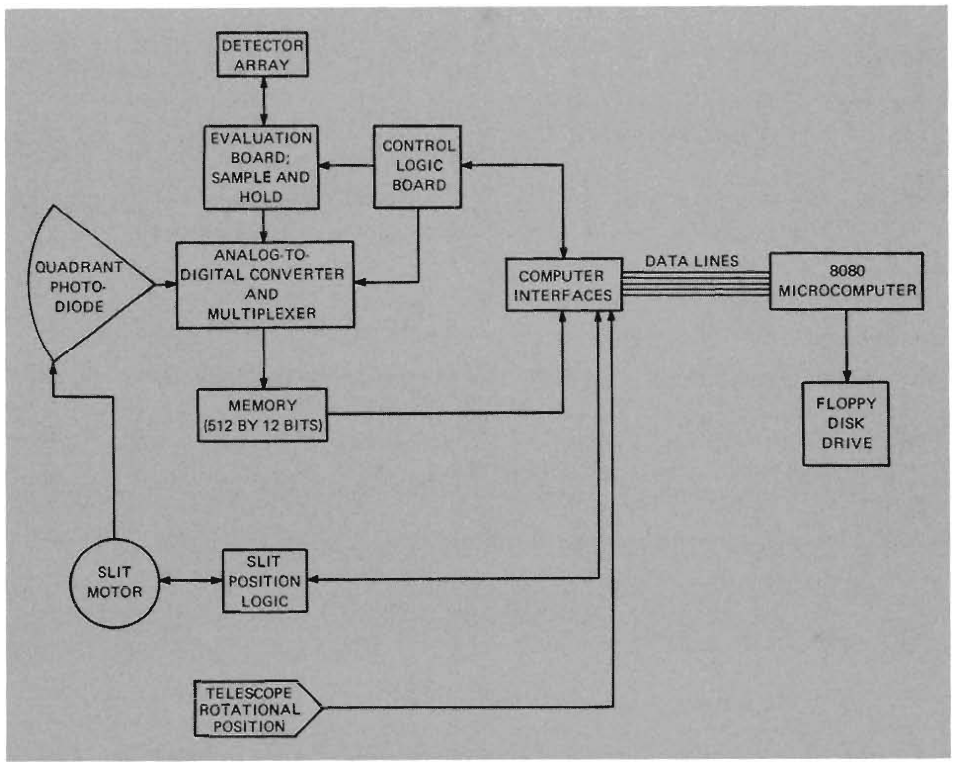

Fig. 26. Block diagram of computer-controlled data-acquisition and storage system for electron temperature experiment. The detector array was read out with Reticon Corporation's evaluation circuitry. Although not ideal for this application, the circuitry provided a signal-to-noise ratio of greater than 100. Data were to be stored in near real time on floppy disks. Computer programs were written in FORTH, a language developed at the University of Rochester.

Infrared Observations of Dust Rings

The F corona and the zodiacal light, a zone of scattered light symmetric about the approximate plane of the planetary orbits, give clear evidence of the presence of dust throughout much of the solar system. These observations also indicate that the dust particles are very fine—only a few micrometers in diameter. Their presence may be a remnant of the formation of the solar system but probably wandering comets have also left a contribution.

Whatever the source, theorists have modeled the fate of the dust once it is deposited in the solar system. The dynamics of the dust particles is influenced by four factors: the sun's gravity, radiation pressure, the Poynting-Robertson effect, and particle evaporation. Calculations including these factors indicate that the dust will spiral in toward the sun but may ultimately settle at particular distances and form broad rings about the sun. Evaporation of the dust may also lead to its being blown outward once again. By determining the radial location of these rings we learn something about the dust's composition because its location depends on its reflectivity and evaporation temperature. Likely compositions include obsidian, silicate-type rock, iron, and perhaps water-ice.

The presence of glowing dust rings at 4, 9, and 20 $R_{\odot}$ and elsewhere has been deduced from observations of infrared emission features (Fig. 27). These emission features are presumably produced as dust particles heat up and evaporate, emitting radiation corresponding to black-body temperatures between 500 and 2000 K. These observations are difficult to make from the

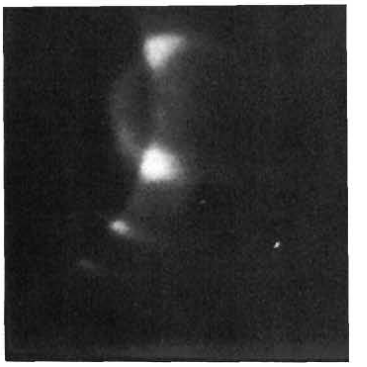

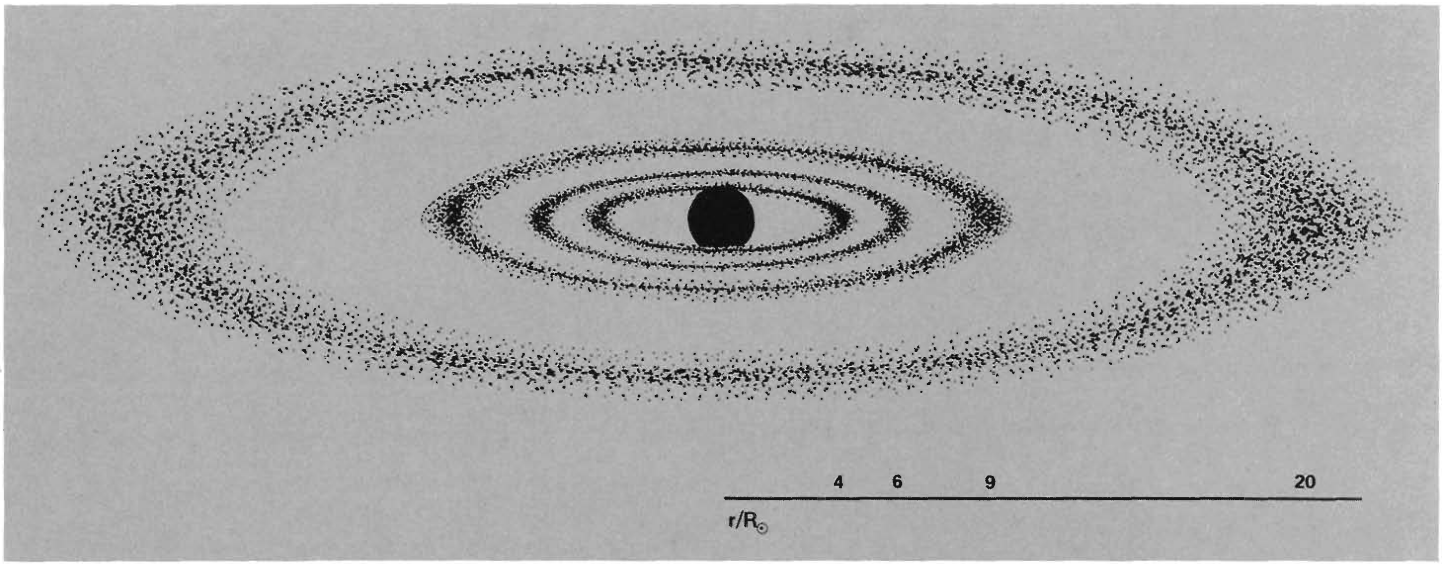

Fig. 27. Approximate radial location and extent of infrared emission features reported by various observers. Only the features at 4 and 9 $R_\odot$ are confirmed.

ground and, with the exception of the feature at 4 $R_\odot$, the existence of these features is in dispute.

From aboard the aircraft during the 1980 eclipse, we made a new attempt to determine the spatial distribution of infrared emission features.

Infrared intensity as a function of distance from the sun was measured at 2.2 μm with an InSb detector, a standard technique, and at ~0.7 μm with a charge-injection-device television camera.

The corona was scanned along the ecliptic (plane of the earth's orbit) out to 50 $R_\odot$ east and west of the sun and at several angles to the ecliptic. The scan pattern was designed to determine the radial location and approximate extent of any dust rings.

Both detection systems worked well and yielded high-quality data. However, tracking errors during totality will severely compromise interpretation of data close to the sun, so we will not be able to confirm the existence of the feature at 4 $R_\odot$. At greater distances, however, these errors have less effect.

Our analyses to date strongly suggest the existence of a dust ring at 9 $R_\odot$, but indicate no other features at greater distances from the sun. Thus we find no feature at about 20 $R_\odot$. A feature at this location, which corresponds to a temperature of ~800 K, had been suggested by E. P. Nye on the basis of ground-level observations at the February 26, 1979, and February 16, 1980, eclipses; however, at both eclipses his observations may have been contaminated by the effects of clouds. Existence of such a feature would be of interest because dust shells with temperatures of ~800 K have been found about some other stars.

Conclusions

Most scientists studying the solar corona believe that a temperature maximum exists near 2 $R_\odot$. Our results indicate that the maximum might be closer to the limb, although some of the Fe XIV emission line broadening can always be attributed to large-scale turbulence or to expansion velocities. However, comparison with proton temperature values from the rocket-borne coronagraph at a few positions in the corona will allow us to determine such velocities if they exist. We can then interpret the rest of our iron emission line data in light of these findings. The fact that many of our 1980 profiles are actually double-peaked indicates large differential mass motions that are probably due to the extremely complex nature of coronal features during maximum solar activity.

Ion temperature gradients measured in 1965 indicated that coronal holes could support solar wind flow. We now have high-resolution data from our 1980 measurements of the residual coronal hole above the sun's south pole to compare with the 1965 results. We will also

be able to analyze temperature gradients and velocity distributions in streamer structures, to determine whether these structures also contribute to solar wind flow.

Our emission line intensity data from several previous solar eclipse observations suggested that collisional mechanisms dominate energy transport in the lower corona out to 2 $R_\odot$. Our high-resolution 1980 data from several streamer structures and one coronal condensation, when combined with electron densities determined from camera-polarimeter measurements, will be a better test of this model.

The possibility of extended wave heating in the corona has become increasingly significant. Our emission line intensity data from the 1973 Concorde flight, which gave 74 minutes of totality, provided tentative evidence for periodic temperature variations, and in 1980 we looked for temporal changes on the sun's west limb by taking a sequence of intensity measurements at 30-second intervals over the 7 minutes of totality. But a more extensive search will be required to establish the dynamics and the extent of plasma heating.

Comparison of the computer-enhanced coronal photographs from five eclipses shows that the corona at the 1980 eclipse exhibited features never before seen, including the umbilical connection of the hydrodynamic eruptive disturbance to the solar surface. This observation calls into question previous speculation, based on Skylab photographs down to 1.5 $R_\odot$, that the connection to the surface was quite broad. Evidently the energy source for some mass eruptions is localized and concentrated. We may learn more about the dynamics at the base of this disturbance once our electron density and Fe XIV data have been reduced.

Our photographic record also shows that nearby streamers respond to the eruption by bending around it, an effect also seen on Skylab photographs but only out to 6 $R_\odot$. The curious shape of long streamers above the sun's south pole suggests that a second eruptive disturbance may also have been in progress at the same time.

Electron densities resulting from our observations agree with other studies in the inner corona, but beyond 4 $R_\odot$ in equatorial regions the density decrease with radial distance is much more gradual than indicated previously. This could have a marked effect on theoretical models of the solar wind.

In summary, we now have collected ion temperature and electron density data at all phases of solar activity except during a deep minimum. Our 1980 data combined with proton temperatures from rocket experiments will provide a focal point for all future analysis. For the first time, we will have an accurate determination of material density, ion temperatures, and nonthermal velocities at several places in the corona. We hope these results will be a basis for more meaningful interpretation of our data throughout the rest of the inner corona ■

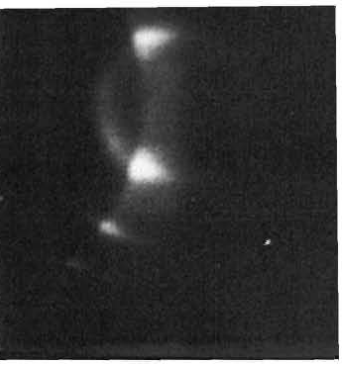

AUTHORS

Donald H. Liebenberg earned his Bachelor of Science in 1954 and his Ph.D. in physics in 1971, both from the University of Wisconsin. He has been a Staff Member at Los Alamos since 1961. His interest in solar physics, which dates to his undergraduate days, led in 1963 to the Laboratory's involvement in observations of total solar eclipses. This activity has resulted in detailed studies over a solar cycle of the physical properties and energy transfer mechanisms of the coronal plasma. During 1967 and 1968 he was Program Director for Solar Terrestrial Research at the National Science Foundation. In 1973 he received a National Science Foundation Grant for observation of a solar eclipse from the French-British Concorde 001. His other research interests include properties of gases at high pressures and laser optics and technology.

Charles F. Keller, Jr., is well known for his involvement in airborne eclipse expeditions, having served as principal investigator of polarization experiments on missions in 1970, 1972, 1973, 1977, and 1980; he was scientific coordinator for missions mounted in 1979 and 1980. After receiving his Bachelor of Arts from St. Vincent College in 1961, he went on to earn a Bachelor of Science in physics from Pennsylvania State University and a Master of Science and Ph.D. in astronomy from Indiana University in 1967 and 1969, respectively. His thesis, "Computer Models of Pulsating Stars Including Radiative Transfer," was produced jointly at Los Alamos and Indiana University. He joined the Laboratory in 1969 and has served as a Staff Member, Assistant Group Leader, and Group Leader of the Diagnostics Design Group of the Field Testing Division. At present he is with the Laboratory's Computer Modeling Group of the Geosciences Division. Keller served as the Field Testing Division's representative on the Director's Computer Advisory Committee, and as the Laboratory's coordinator of computer modeling for the Department of Energy's Atmospheric Studies over Complex Terrain (ASCOT) Program. He is a member of the American Astronomical Society and its Solar Physics Division.

Further Reading

E. N. Parker, *Interplanetary Dynamical Processes* (Wiley-Interscience, New York, 1963).

D. E. Billings, *A Guide to the Solar Corona* (Academic Press, New York, 1966).

H. Zirin, *The Solar Atmosphere* (Blaisdell Publishing Co., Waltham, Massachusetts, 1966).

J. C. Brandt, *Introduction to the Solar Wind* (W. H. Freeman and Co., San Francisco, 1970).

R. G. Athay, *The Solar Chromosphere and Corona: Quiet Sun* (D. Reidel Publishing Co., Dordrecht, Holland, 1976).

J. B. Zirker, Ed., *Coronal Holes and High Speed Wind Streams* (Colorado Associated University Press, Boulder, 1977).

E. N. Parker, *Cosmical Magnetic Fields: Their Origin and Their Activity* (Clarendon Press, Oxford, 1979).

J. B. Zirker, "Total Eclipses of the Sun," Science **210**, 1313-1319 (1980).